Formation & Evolution of Planetary Systems (FEPS)

FEPS Data Explanatory Supplement

Version 3.0

15 December 2005

Revision History

VERSION	DESCRIPTION	DATE
1.0	Initial Release	15 Sept 2004
1.1	Revised for October 17 SSC release	17 Oct 2004
2.0	Add MIPS 160, IRS Hi-Res, IRAC & MIPS Images Add V&V section and discussion of photometry	15 May 2005
2.1	Corrected bad table labels in S7, error in Table 7.2	15 Sept 2005
3.0	Revised for DR3, updated IRAC, MIPS & IRS	15 Dec 2005

Citation Instructions

The Explanatory Supplement version v3.0 was compiled by the following FEPS data team members:

Dean C. Hines, John M. Carpenter, Jeroen Bouwman, Jinyoung Serena Kim, Murray D. Silverstone, Ilaria Pascucci, Michael R. Meyer, Martin Cohen, John Stauffer, Betty Stobie, Dan Watson

In publications, refer to this document as:

Hines, D.C. et al. 2005, "FEPS Data Explanatory Supplement," Version 3.0, (Pasadena: SSC).

Questions regarding this document should be directed to the *Spitzer* Science Center.

The FEPS Science Team

Principle Investigator (PI): Michael R. Meyer (Steward Obs., University of Arizona)

Deputy PI's: Dana Backmann (NASA-Ames/SOFIA) & Lynne Hillenbrand (CalTech)

Co-Investigators: Steve Beckwith (STScI), Jeroen Bouwman (MPIA Heidelberg), Tim Brooke (JPL), John Carpenter (CalTech), Martin Cohen (UC-Berkeley), Uma Gorti (UC-Berkeley), Thomas Henning (MPIA Heidelberg), Dean Hines (Steward), David Hollenbach (NASA-Ames), Jinyoung Serena Kim (Steward), Jonathan Lunine (LPL), Joan Najita (NOAO), Ilaria Pascucci (Steward), Renu Malhotra (LPL), Eric Mamajek (Steward), Amaya Moro-Martin (Steward), Pat Morris (SSC), Deborah Padgett (SSC), Jens Rodmann (MPIA Heidelberg), John Stauffer (SSC), Betty Stobie (Steward) Murray Silverstone (Steward), Steve Strom (NOAO), David Soderblom (STScI), Dan Watson (Rochester), Stuart Weidenschilling (PSI), Sebastian Wolf (MPIA Heidelberg), and Erick Young (Steward).

Information about the FEPS project can be found on the team website:
http://feps.as.arizona.edu/

Table of Contents

REVISION HISTORY II
CITATION INSTRUCTIONS III
THE FEPS SCIENCE TEAM III
TABLE OF CONTENTS IV
1 INTRODUCTION 1
1.1 Purpose of This Document 1
1.2 The FEPS Legacy Science Program 1
1.3 Executive Summary of FEPS Enhanced Data Products 1
1.3.1 Staged Delivery 2
1.3.2 Primary Data Products 2
1.4 The FEPS V3.0 Release 3
1.5 Cautionary Notes and Caveats for FEPS Data Release V 3.0 3
2 FEPS SAMPLE SELECTION 6
3 THE AORS & THE SSC PIPELINED DATA 7
4 KURUCZ MODEL ATMOSPHERES 8
5 INFRARED ARRAY CAMERA (IRAC) DATA 9
5.1 IRAC Data and the SSC Pipeline Products 9
5.2 IRAC Point-Source Photometry 9
5.3 Photometric Uncertainties & Calibration, Wavelengths and Color Corrections 10
5.4 IRAC Mosaiced Images 11
6 INFRARED SPECTROGRAPH (IRS) DATA 12
6.1 IRS Data and Pipeline Products 12
6.2 Low Resolution Spectra 12
6.2.1 Spectral Extraction 12
6.2.2 Flux Calibration 14
6.2.3 Uncertainty Estimates 23
6.2.4 Order Stitching 26
6.3 IRS High Resolution Spectra 26
6.3.1 Data Reduction of the Sources with Associated Sky Observation 27
6.3.2 Line Fluxes and Upper limits 31
6.3.3 Caveats (Needs Revision) 32
7 MULTIBAND IMAGING PHOTOMETER FOR SPITZER (MIPS) DATA 33

7.1 MIPS Data and DAT pipeline....33
7.1.1 The Si:As 24μm Data....33
7.1.2 The Ge:Ga 70μm and 160μm Data....33
7.2 MIPS Point-Source Photometry....34
7.3 Photometric Calibration, Wavelengths and Color Corrections....35
7.4 MIPS Mosaic Images....35
7.4.1 24μm Mosaics....36
7.4.2 70μm & 160μm Mosaics....36
8 ENSEMBLE CHARACTERISTICS OF THE FEPS V3.0 DATA RELEASE....37
8.1 IRAC & MIPS Photometry....37
8.1.1 Internal uncertainties in the IRAC photometry....38
8.1.2 Internal uncertainties in the MIPS 24μm photometry....40
8.1.3 Internal uncertainties in the MIPS 70μm and 160μm photometry....42
8.1.4 Calibration Uncertainties....43
8.2 IRS Calibration....45
8.3 Cross-Calibration....47
9 ANCILLARY DATA PRODUCTS....47
9.1 10μm Photometry....47
9.2 Millimeter and Sub-Millimeter Measurements....47
10 REFERENCES....48
11 APPENDIX A....49
12 (INCOMPLETE) ACRONYM LIST....50

1 Introduction

1.1 Purpose of This Document

This document describes the high-level data products that the *Spitzer* legacy science program titled the Formation and Evolution of Planetary Systems (FEPS) has produced and delivered to the *Spitzer* Science Center (SSC) for distribution to the larger astronomical community. It contains the observational program, including the sample selection, basic observing strategy, and the steps used to create the enhanced data products for each instrument and mode. This version (V.3.0) is released to accompany the Dec, 2005 FEPS data product release. Readers should refer to Section 1.5 for important caveats on the current FEPS data products release. Readers should also refer to Section 8, which discusses the ensemble characteristics of the data including a quantitative evaluation of the photometric uncertainties.

1.2 The FEPS Legacy Science Program

The Formation and Evolution of Planetary Systems (FEPS) *Spitzer* legacy science program will trace the evolution of planetary systems at ages ranging from: (1) 3-10 Myr when stellar accretion from the disk terminates; to (2) 10-100 Myr when planets achieve their final masses via coalescence of solids and accretion of remnant molecular gas; to (3) 100-1000 Myr when the final architecture of solar systems takes form and frequent collisions between remnant planetesimals produce copious quantities of dust; and finally to (4) mature systems of age comparable to the Sun in which planet-driven activity of planetesimals continues to generate detectable dust. Our strategy is to use carefully calibrated spectral energy distributions (SEDs) and high-resolution spectra to infer the radial distribution of dust and gas content of disks surrounding a sample of 328 sun-like stars distributed uniformly in log-age from 3 Myr to 3 Gyr.

This Legacy program will provide: (1) insight into problems of fundamental scientific and philosophical interest; (2) enhanced internal calibration for comparison with standard *Spitzer* data products; (3) new simulations of the dynamical history of forming solar systems; and (4) a rich database to stimulate follow-up observations with *Spitzer*, with existing and future ground-based facilities, and later with *SIM*, *JWST*, and *TPF*.

1.3 Executive Summary of FEPS Enhanced Data Products

It is the charge of all the *Spitzer* Science Legacy teams to develop a comprehensive observational program to address a key area of observational Astronomy that is facilitated by the *Spitzer Space Telescope (Spitzer)*, and that will provide a large dataset that will serve as a legacy for archival research and support of future science missions. The program also includes ancillary data that support the primary science theme. In addition to coordinating the observations, the Legacy Teams shall deliver data products enhanced beyond the routine pipeline products provided by the SSC legacy science archive. For FEPS, these products include photometry measured from processed images and one-dimensional spectra of all targets, plus supporting uncertainties and quality assessments. These products are intended to be used directly for conducting science investigations without further refinement.

1.3.1 Staged Delivery

The FEPS data products will be released incrementally at approximately six-month intervals phased with major updates of the SSC pipeline reprocessing and updated calibration. Since many objects in the FEPS sample have not been observed in time for the first data release in October, 2004 (Stage I), and several may not have complete instrument coverage until Spring 2005, we anticipate that the September 2005 (Stage III) release will provide the first products representing the complete FEPS sample.

October 2004 — Stage I presents the Pointed Observations Photometric Catalog (POPC V1.1) containing *Spitzer* photometry and a IRS low resolution spectral atlas for 33 stars. Kurucz model photospheres are also delivered.

May 2005 — Stage II will provide the products outlined in Stage I for newly observed targets plus updates to the products delivered previously. Updates will include, but are not restricted to, improved measurement uncertainties and refined absolute calibration. Stage II will also provide the first high resolution (R~600: 9.9-37.2μm) IRS spectra and flux measurements for selected emission lines. Stage II will contain the first release of mosaicked images from IRAC and MIPS.

December 2005 — Stage III will provide the products outlined in Stage II for newly observed targets plus updates to the products delivered previously. Stage III is anticipated to be primarily an update and expansion to Stage II, since we expect to have obtained all of the primary FEPS observations by this date.

Spring 2006 — Stage IV: Final Product Delivery — This will be the final formal release of FEPS legacy data products to the SSC. We anticipate that by this date, the instruments and calibrations will have achieved a high level of maturity and that our Stage IV data products will constitute the complete FEPS Legacy Science Product.

1.3.2 Primary Data Products

A comprehensive list of all of the primary data products are described below. The primary enhanced data products produced for stars in the FEPS sample are:

1) **Pointed Observations Photometric Catalog (POPC)**
    a. Flux densities for IRAC (3.6, 4.5, 5.8 and 8.0μm) and MIPS (24, 70, & 160μm) [5.8 and 160μm observations will not be available for all targets]
    b. Ancillary data for select targets via published data tables
        i. (Sub)-millimeter Continuum Photometry
        ii. 10μm Magellan Photometry
    c. Stellar properties to specify the stellar photosphere
2) **IRS Low Resolution Spectral Atlas**
    a. Extracted low resolution (R~64-128) IRS spectra from 7.4 – 38μm for all stars
    b. Extracted low resolution (R~64-128) IRS spectra from 5.2 – 38μm spectra for 3-30 Myr stars
3) **Photospheric models**
    Models of the stellar photosphere fit to short wavelength photometry, and extended through the *Spitzer* wavelengths

4) **Mosaicked IRAC and MIPS images**
   Image atlas
5) **IRS High Resolution Spectral Atlas**
   a. R~600 spectra over 9.9-37.2μm for select stars
   b. Line measurements for selected emission lines within these spectra

1.4 The FEPS V3.0 Release

The FEPS V3.0 data release contains data obtained as part of the FEPS *Spitzer* survey. The current release contains:

- Table of aperture photometry for 291 stars in the IRAC 3.6, 4.5 and 8μm bands, plus MIPS 24, 70 and 160μm bands
    - IRAC 5.6μm band photometry is available for 5 stars
    - MIPS 160μm band photometry is available for 36 stars
    - Tables are formatted as IPAC Tables
    - For each object we list: Name, RA & DEC in decimal degrees, aperture photometry in mJy and the "internal" (precision) uncertainty of the measurement. We also supply data quality flags for the Ge:Ga array data at 70 and 160μm. Details of the uncertainty calculations are presented in Section 7.
- FITS images for all IRAC and MIPS bands observed for each star
- IRS Spectra
    - Low resolution IRS spectra (R~64-128) from 7.4 –38μm for 216 stars
    - Low resolution IRS spectra (R~64-128) from 5.2 –38μm for 75 stars
    - High resolution IRS spectra for 14 stars
- Kurucz model photospheres are also delivered for all 291 stars.

1.5 Cautionary Notes and Caveats for FEPS Data Release V 3.0

The V1.1 and V2.0 data releases contained several caveats that have since been mitigated. The reader is referred to the Explanatory Supplements V1.1 & V2.1 for details. Herein we will only describe caveats pertaining to the current data release, V3.0.

While the FEPS team has made every effort to ensure the quality of the data products, we also remind the users that the calibration, data pipelines and data reduction procedures are still

evolving. Descriptions of SSC pipeline and data issues can be found on the SSC website.[1] Some details can be found in the sections of this document that describe the individual data products for each instrument mode.

Not all of the eventual FEPS data products are released at this Stage (see Section 1.3.1). In particular, this release (V3.0) contains low resolution spectra, and IRAC and MIPS photometry for 291 of the 328 stars in the total FEPS sample: 17 stars were observed as part of a GTO program and the data are not yet available, and the remaining 20 stars either did not have data available for all three instruments or there were problems with the data (e.g., mis-pointing for IRS low resolution). In addition, 14 high resolution spectra are released. Finally, only 36 stars in this release have MIPS 160μm photometry and images, since only a subset of the FEPS sample was observed at this wavelength.

SSC Pipeline: The data products in the December 2005 delivery are based on *Spitzer* products processed through the SSC pipeline. The MIPS data were processed with S10.0.3 and S10.5.0. The IRAC data were processed with S11.4.0. Since the MIPS data are processed through the Data Analysis Tool (DAT) supplied by the MIPS instrument team, the pipeline products are only necessary for the pointing reconstruction, which has not changed between pipeline versions. The IRS data were all processed through the S12.0.2 pipeline.

IRS: For V3.0 we have additionally implemented fringe removal for the LL1 module.

MIPS: All data produced by MIPS are reduced from raw form using the Data Analysis Tool (DAT) developed by the MIPS Instrument Team at the University of Arizona (Gordon et al. 2005). This completely by-passes the current SSC pipeline. Therefore, users cannot reproduce our results using the currently available SSC pipeline products. Future improvements of the SSC pipeline should produce products of equal quality to that produced by the DAT (the 24μm products produced by both are already nearly indistinguishable). Individual frames from the two MIPS Ge:Ga arrays (70μm and 160μm) still suffer from instrumental minor artifacts as a function of position on the array. However, these have been minimized by combining the dithered images, and using the time history of the sensitivity imbedded in each image to make corrections before performing photometry (Gordon et al. 2004, 2005).

Calibration of the Data Products Relative to Best-Fit Kurucz Models: We have compared our measured IRAC & MIPS photometry and spectra with the delivered Kurucz stellar atmosphere models that best fit the UV, optical and near-IR photometry. We have also done this for the IRS spectra using four synthetic band-passes, two of which correspond with the IRAC 8.0μm and MIPS 24μm bands. This latter synthetic photometry enables us to evaluate the cross calibration between the three instruments. We note that there are some systematic offsets between our model fluxes and the observed fluxes. Investigators are encouraged to read the information in Section (8), which describes the characteristics of the V3.0 dataset as a whole, and provides the details for our final assignment of the delivered photometric uncertainties.

[1] http://ssc.spitzer.caltech.edu

Color Corrections: The IRAC and MIPS photometric measurements have not been "color corrected." The measured flux densities assume a spectral energy distribution (SED) that is flat ($F_\nu = \nu F_\nu = \text{const}$) across the band passes for IRAC, and a 10,000 Kelvin black body across the band passes for MIPS. Objects with SEDs differing from these assumptions require that their flux densities be corrected. These color corrections are expected to be smaller ($\leq$ 15% in the most extreme cases for very cold sources in MIPS 24μm than the current calibration uncertainties. Currently tabulated color-corrections for the two instruments can be found in the Data Handbooks available through the SSC.

2 FEPS Sample Selection

The main goal in FEPS is to follow the evolution of circumstellar dust around solar-type stars, first as the primordial circumstellar material dissipates in the 3-30 Myr time scale and then as secondary or "debris" disks form as byproducts of completed planet formation after ~30 Myr. Our source list thus consists of young near-solar analogs, stars ranging in mass from 0.8-1.2 Msun, and spanning ages 3 Myr to 3 Gyr (our Sun is 4.5 Gyr old). The stars are drawn from three recently assembled samples.

First, Soderblom et al. (2003) have produced a well-characterized set of ~5000 solar-type stars spread over the entire sky (see also Henry et al. 1996) having parallaxes that place the stars within 60 pc, (B-V) colors between 0.52 and 0.81 (F8-K0 spectral types), and location in the HR-diagram within 1.0 mag of the solar-metallicity Zero-Age Main Sequence. The sample includes stars with ages up to several Gyr old, but with a bias against the oldest disk stars due to disk heating (causing the scale height to be larger for the older stars). From this catalog we have selected a sample of stars whose ages based on the R'_{HK} chromospheric activity index are ~100 Myr to 3 Gyr. However, since earth is located more than 100 pc from the nearest sites of recent star formation, our immediate solar neighborhood is deficient in stars with ages younger than a few 100 Myr and hence the volume limit was extended in order to identify large enough samples of young stars for this project.

Second, therefore, we have conducted a new (e.g. Mamajek et al., 2002) and literature-based examination to identify stars whose ages are in the range 3-100 Myr. These were selected as having (B-V) colors between 0.58 and 1.15 or spectral types G0-K0, strong x-ray emission, kinematics appropriate for the young Galactic disk, and high lithium abundance compared to the 120 Myr old Pleiades.

Young stars are copious coronal x-ray emitters and a large body of literature demonstrates the connection between x-ray emission, chromospheric activity, stellar rotation, and age. The surface density distribution of x-ray sources detected by the ROSAT all-sky survey reveals a concentration of objects coincident with Gould's Belt, a feature in the distant solar neighborhood (50-200 pc) comprised of an expanding ring of atomic and molecular gas of which nearly all star-forming regions within 1 kpc are a part. These x-ray sources are thought to be the dispersed low-mass counterparts to a series of 1-100 Myr-old open clusters and OB associations that delineate Gould's Belt (e.g. Torra et al. 2000; Guillot 1998). Proper motion data enable us to select the nearest of these young, x-ray-emitting stars with space motions consistent with those of higher mass stars having measured parallax, and hence estimate their distances. As was true for the $d < 50$ pc sample discussed above, follow-up optical spectroscopy of these x-ray plus proper motion-selected stars is used to confirm youth and determine photospheric properties. A total of ≈600 field stars are x-ray-selected candidates.

Finally, stars in nearby well-studied open clusters [IC 2602 (55 Myr), Alpha Per (90 Myr), Pleiades (125 Myr), Hyades (650 Myr)] serve to "benchmark" our field star results by providing samples nearly identical in age, composition, and birth environment. We considered all known members of these clusters meeting our targeted mass / B-V color / spectral type range.

From this large parent sample, stars were selected for observation with *Spitzer* if they met all of the following additional criteria. The criteria were chosen to ensure sufficient signal-to-noise on

the stellar photosphere at 24μm with *Spitzer* and our ability to accurately characterize the underlying photosphere both observationally and with stellar models.

- K< 10 mag (young x-ray selected and cluster samples) or < 6.75 mag (older Hipparcos and R'HK selected sample)
- 24μm background < 1.70 mJy/arcsec^2 (young x-ray selected and cluster samples) or < 1.54 mJy/arcsec^2 (older Hipparcos and R'HK selected sample)
- 70μm background < 0.76 mJy/arcsec^2
- Galactic latitude away from the plane, |b| > 5˚ (stars in IC 2602 do not meet this criterion)
- available 2MASS JHK photometry with low errors and no flags
- no projected companions in the 2MASS survey closer than 5 arcsec
- no projected companions in the 2MASS survey closer than 15 arcsec unless they are *both* bluer in J-K *and* fainter in K by > 3 mag than the *Spitzer* target

Generally speaking, these criteria were applied uniformly to our parent sample; in the cases of a few exceptional stars some criteria were violated, though only slightly. Targets already included in *Spitzer* GTO programs were then removed from the source list. Also, in general, stars identified through spectroscopy or high resolution imaging in literature published through March 2001 as being binary with companions closer than 2 arcseconds were removed. These were all either spectroscopic binaries or visual binaries with small delta magnitudes. Subsequent investigation using AO imaging have uncovered some additional binary systems with large delta magnitudes remaining within the FEPS sample. The remaining binaries are discussed in detail by Metchev et al. (2005).

Finally, amongst the stars in our parent sample older than ~600 Myr, approximately 1/2 were removed from our program in order to even out the age bins and bring the observing program within the allocated number of *Spitzer* hours. Our final target list for observations with *Spitzer* and ground-based ancillary programs consists of 326 solar-type stars distributed uniformly in log-age between 3 Myr and 3 Gyr. Approximately 60 of these are members of the open clusters IC 2602, Alpha Per, Pleiades or Hyades. Based on pre-*Spitzer* spectral energy distributions assembled from the literature, 2MASS, *IRAS*, and ancillary observations conducted to date, several (10-15) of the youngest stars in our program show some hint of circumstellar material.

3 The AORs & The SSC Pipelined Data

The AOR commands that specify our program can be found using SPOT[2] to "View Program," and entering our Program Identification Number (PID = 148). The SSC pipelined data products

[2] http://ssc.spitzer.caltech.edu/propkit/spot/

can be accessed through the LEOPARD archive browser under the "Popular Products" menu and using PID = 148. We note below a few characteristics of the SSC archived data that should be kept in mind when browsing and retrieving the SSC pipelined products.

Because all of the FEPS stars are bright in the IRAC bands, all of the IRAC observations were obtained with sub-array mode. The first five FEPS objects (as part of the early verification program) were observed in all four IRAC bands. All other targets were observed in only three bands (3.6μm, 4.5μm, 8μm). Note that even though the 5.6μm channel was not observed for these targets, data in that band associated with some of the other FEPS stars does appear in the SSC data archive. This is because parallel data are obtained for the off-source field for longer sub-array sample times (see IRAC Manual). These parallel data do not contain our program targets, and thus we have made no attempt to process them further.

Low resolution IRS spectra covering the entire wavelength range are available for the first five FEPS verification targets and objects younger than 30 Myr. For all other objects in the FEPS sample, the SL2 module was not observed, so the wavelengths from 5.2 – 7.4μm are not present for these objects.

High resolution IRS data are currently planned for ~50 stars.

MIPS 24μm and 70μm data were obtained for all stars in the FEPS sample that were not otherwise observed by Spitzer GTOs or other Legacy Teams.

4 Kurucz Model Atmospheres

Model atmospheres for each of the 150 FEPS stars are included with the FEPS V2.0 data release. The expected photospheric emission for each star was determined by fitting Kurucz model atmospheres with convective overshoot to published optical photometry including, if available, Johnson *BV*, Stromgren *vby*, Tycho *BV*, Hipparcos H_p, Cousins *RI* and 2MASS JHK_s measurements. Predicted magnitudes in each filter were computed by multiplying the Kurucz model with the combined system response of the filter, the atmospheric transmission (for ground-based observations), and the spectral response function of the detector as outlined in a series of papers by Cohen et al. (2003a,b; and references therein). The Johnson *U* and Stromgren *u* filters were excluded from the model fits because the observed photometry shows large deviations from the model values explained in part by chromospheric activity common in young late-type stars. The best-fit Kurucz model was computed in a least squares sense with the effective temperature and normalization constant as free parameters. The metallicity was fixed at [Fe/H] = 0.0 and the surface gravity at $\log(g) = 4.5$. Extinction for each star was also a fixed parameter. The parameters for each model are contained within the headers of each Kurucz model file.

5 Infrared Array Camera (IRAC) Data

The IRAC instrument provides images in four bands (3.6, 4.5, 5.6 & 8μm). Because the FEPS targets are bright at these bands, all of the FEPS IRAC observations were performed using the subarray mode. Also, the 5.6μm band was only used to observe the first five verification targets (Meyer et al. 2004), and was subsequently dropped for the rest of the sample.

5.1 IRAC Data and the SSC Pipeline Products

The FEPS targets were observed in the IRAC subarray mode (32x32 pixels) at frame-times of 0.02, 0.1, or 0.4 seconds, using the "4 point-random" dither pattern at the medium dither scale, in IRAC channels 1, 2, 4 (the 5 verification targets were also observed in IRAC channel 3). At each of the 4 dither positions, 64 images were taken at the same frame-time in each channel. The data frames were processed through the SSC pipeline to produced Basic Calibrated Data (BCD) images. Each BCD image contained 64 images of the object. The 4 dithers resulted in 4*64 = 256 images of the object, in each channel.

5.2 IRAC Point-Source Photometry

Each of the images were photometered using the IRAF task PHOT which is part of the APPHOT package. Please see Appendix A for the parameter values used for the PHOT task.

All of the delivered IRAC photometry used a 2-pixel radius target aperture, centered on the location of a Gaussian fit to the PSF, supplying the FWHM measured from the over-sampled PSFs available on the SSC website[3], and then re-scaled to the IRAC native pixel scale. Table 5.1 lists the FWHMPSF values used in the IRAF APPHOT DATAPARS parameter set (see Appendix A) to determine the centroids for individual image photometry

Table 5.1: FWHM Parameters

Channel	FWHM [Pixels]
1	1.53
2	1.41
3	1.62
4	1.88

The background annulus was taken from 10 pixels to 32 pixels. In most cases, this annulus circumscribes the 32x32 array and thus uses all pixels outside of the 10-pixel radius. An area and scale conversion was used to transform the pixel values from the image units of MJy/Ster to mJy/pixel, using the pixel scale in the image headers.

[3] http://ssc.spitzer.caltech.edu/irac/psf.html

Multiplicative aperture corrections were derived to correct the radius = 2 pixel photometry to the radius = 10 pixel standard for IRAC absolute calibration data, for the 3.6μm, 4.5μm, and 8.0μm measurements from the sample of observed FEPS targets. These corrections were computed from the ratio of the measured flux with target aperture radius = 2 pixels to that measured with target aperture radius = 10 pixels, both using a background derived from the annulus from 10 to 32 pixels, as described above. For one of the four dither positions, many of the radius = 10 pixel target apertures fell off the 32x32 pixel subarray; thus that dither was excluded from the aperture correction determination. A median and standard deviation were calculated from the 64 measurements at the remaining three dither positions for each target. The weighted mean aperture correction was computed from the medians of the ratios between the aperture measurements weighted by the root-mean-square of the standard deviations of the measurements in each of the two apertures. The aperture corrections and uncertainties computed from the weights are given in Table 5.2.

The aperture correction for the 5 targets measured at 5.8μm were performed using the values published in the Infrared Array Camera Data Handbook v. 2.0 Table 5.7, for radius on source 2.0 pixels, and background annuli of 10 to 20 pixels. The size and shape of the subarrays are such that the background annulus specified by the Data Handbook could not be replicated exactly. Thus all pixels outside of a 10-pixel radius were used, as described above. The uncertainty in this aperture correction was assumed to be 2%, as described in the text of the Infrared Array Camera Data Handbook v. 2.0, page 44.

Table 5.2: IRAC Aperture Corrections

Channel	Aperture Correction	Uncertainty
1	1.224	0.0009
2	1.222	0.0015
3	1.363	0.02
4	1.574	0.0029

The Channel 1 data were corrected for the pixel phase effects using the formula listed in the Infrared Array Camera Data Handbook v. 2.0, eqn. 5.12 (page 43), with the Gaussian centroids computed with the PHOT routine as described above..

5.3 Photometric Uncertainties & Calibration, Wavelengths and Color Corrections

The uncertainties in the measured photometry of the IRAC images is described in detail in Section (8). The photometric calibration uncertainty of IRAC is currently advertised by the SSC to be 10% (1σ) in all bands. We note that the IRAC calibration is tied to the "weighted average" wavelengths of each filter/detector combination, which are (3.548μm, 4.492μm, 5.661μm, 7.87μm). The photometry reported in the FEPS data products do not have a color-correction applied. The IRAC team assumes that the correction = 1.000 for νF_ν = const. Users are cautioned that a color correction should be applied based on the tables available from the SSC

(Sec. 5.2 of the IRAC Data Handbook). Note that these tables assume black-bodies and power-laws, not stellar models.

5.4 IRAC Mosaiced Images

A median image was computed from the 64 images at each dither position in each channel, using the IRAF routine IMCOMBINE, with the 3-sigma clipping factor for both low and high sigma clipping. A Gaussian centroid was computed for the target in each median image using the PHOT routine and the channel-specific FWHMs listed above. The offsets between the dither images were computed, then rectified by subtracting the most negative shifts in X and Y. The rectified shifts were then rounded and subtracted to compute a whole-pixel shift and the smallest fractional pixel shift. The fractional pixels shifts were applied using the IRAF routine IMSHIFT, using the linear interpolation algorithm. The four fractional-pixel-shifted dither images for each target in each channel were then shifted by whole-pixel values and combined using the IMCOMBINE routine using the median combination algorithm. None of the images were rescaled or distortion corrected.

6 Infrared Spectrograph (IRS) Data

Observations using the Infrared Spectrograph (IRS) low resolution modules (R~64-128) from 7.4 –38μm will be obtained for all objects of the FEPS sample[4]. Observations using the Short-Lo 1 (SL1) module (5.2 – 7.4μm) were obtained for the first five validation targets and for all stars with ages in the range of 3-30 Myrs. Dropping the SL2 observations for the older stars was deemed acceptable for older objects because no spectral features other than from the stellar photosphere are expected over this wavelength region. The time saved by not using the SL2 for all targets allowed for longer integration times for instrument modes that were found to be underperforming compared with pre-launch estimates.

6.1 IRS Data and Pipeline Products

The IRS data are first processed through the SSC pipeline to remove instrumental artifacts including dark current, droop. For the data delivered to the SSC as enhanced data products we use as a basis the intermediate "droop" data product, processed trough pipeline version S12.0.2, which was made available in the SSC data archive on time of this data delivery.

6.2 Low Resolution Spectra

6.2.1 Spectral Extraction

The SMART reduction package developed by the IRS Instrument Team at Cornell (Higdon et al. 2004) for details on this tool and extraction methods) is used to extract the spectra. We use the droop intermediate data product delivered by the SSC pipeline from which we extract our spectra. As a first step, we correct for the background emission and stray-light by subtracting images of the two slit positions at which a target is observed for each module and order. This results in a set of images containing a positive and negative source in each observed order.

For the spectral extraction we use a straight-sided (boxcar) aperture limiting the extraction area around the positive source in the background corrected images. Since all observations in the FEPS legacy program use high accuracy peak-up, the pointing of *Spitzer* is good to within 0.4" radius (1 sigma), we opted to fix the position of the aperture of each spectral order, and not to perform source profile fitting to determine the source position for each individual source during extraction. We have checked the accuracy of the positioning of the FEPS targets in the slit and the exact source location at each nod position. As an example, Figure 6.1 shows the positive and negative source profiles in the SL1 and LL2 orders, derived from the background corrected image of the 16 calibration sources listed in Table 6.2. We found that the source positioning has the expected 0.4" (1 sigma) pointing accuracy, but that the targets are not positioned exactly on the 1/3-2/3 position along the slit. Table 5.1 lists the center position of the extraction apertures, taken to be the mean source position of our calibration stars. The width of each aperture is determined by two quantities: (1) the maximum size of the PSF in each order; and (2) the pointing accuracy. The width of each aperture is chosen such that 99% of the source flux is

[4] A few stars will be observed as part of other science programs. This data will be analyzed by the FEPS team and incorporated into our released products when the proprietary period on the observations has expired.

within the aperture. To determine the maximum size of a point source for each module, we have performed source profile fitting assuming a sinc profile. Taking also the positioning constraints into account, the apertures are widened an additional 2.4" (6σ), to ensure that the entire source is always positioned within in the aperture. Table 6.1 lists the resulting aperture widths in pixels, taking a 1.85" and 5.08" pixel scale for the short-low and long low modules, respectively.

Before extraction, pixels marked in the bmask file with bit 9 or higher set and all NaN's in each image separately are replaced with the average pixel value of a 6 pixel box surrounding the dead pixel. The method we apply for finding the mean pixel value resembles Nagao & Matsuyama filtering and ensured edge preservation in the source region of our spectral images.

After the extraction of the spectrum for each nod position and cycle, a mean spectrum over all slit positions and cycles is computed for each individual order. The orders are then combined. In the regions where the spectra of the individual orders overlap the fluxes are replaced by the mean flux value at each wavelength point. The quoted uncertainties are the 1 sigma standard error in the mean of the distribution of data points used to calculate the mean spectrum over all cycles and nod positions, modified to include the errors of the calibration (See also the next sections for more details on the error analysis).

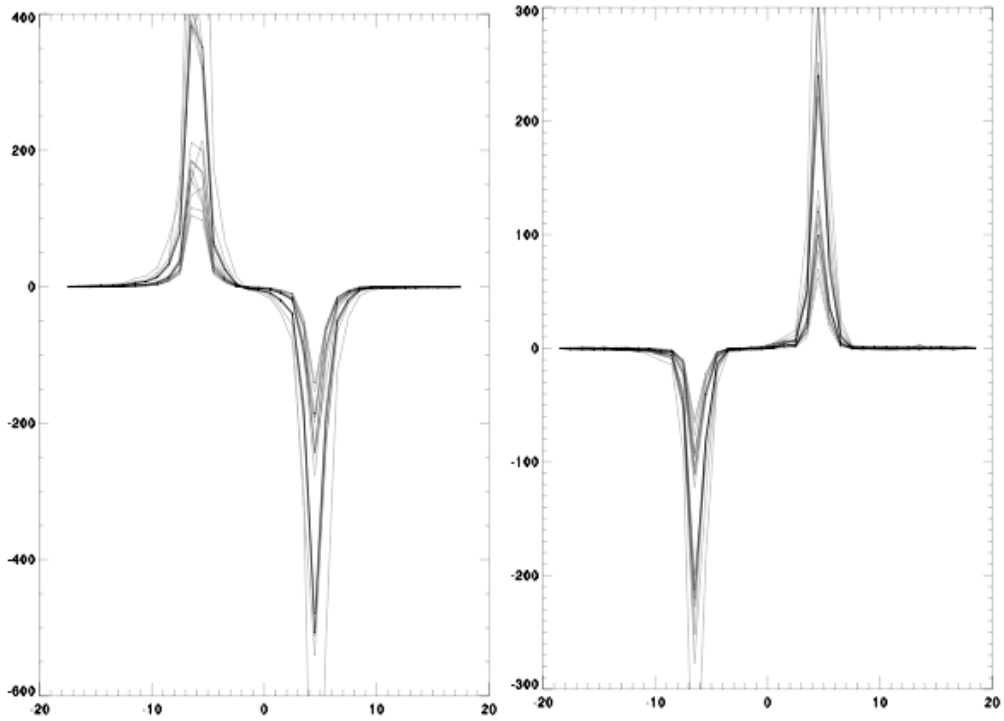

Figure 6.1 Source profiles in the SL1 (left figure) and LL2 (right figure) order for the calibration targets as listed in Table 6.2. On the x-axes the position in pixels relative to the central position is plotted, on the y-axis flux (arbitrary units).

6.2.2 Flux Calibration

The FEPS legacy program provides us with an unique opportunity to derive a good flux calibration for low mass main-sequence stars, since it contains observations of targets for which no circumstellar emission has been detected at IRS wavelengths, resulting in a large number of observations of purely stellar photospheres. To calibrate the extracted spectra and to remove systematic instrumental artifacts, we use order-based spectral response functions (RSRFs), which are the extracted spectra of the standards divided by the corresponding stellar model. We derived the RSRFs from a set of 16 calibration stars for the SL1, and LL orders, and from a separate set of 10 stars for the SL2 and SL3 orders, as listed in Tables 6.2 and 6.3.

We have selected these stars on the following criteria:

(1) The flux ratios of the synthetic photometry points at 8, 13, 24 and 33μm are within one sigma of the expected position for a stellar photosphere.

(2) No evidence for a IR excess in the IRS spectra based on deviation from the adopted Kurucz model for that star.

(3) Clean spectra i.e. no artifacts in the spectra due to cosmic ray hits, hot or dead pixels, pointing problems, etc.

(4) The best available SNR for the specific order and ramp time ensuring good quality RSRFs.

Table 6.1: The resulting position and width of the extraction apertures used for all well positioned sources. For each module, order and slit-position the width of the aperture in pixels and the aperture center relative to the central pixel of each order for both nod positions are given.

Order	**Maximum wavelength (micron)**	**Aperture width (pix)**	**Aperture center nod position 1**	**Aperture center nod position 2**
SL2	7.6	6	-5.61	4.49
SL3	8.6	6	-5.66	4.43
SL1	14.5	6	-6.13	4.52
LL2	20.8	5	4.86	-6.13
LL3	21.6	5	4.75	-6.35
LL1	37.0	5	5.4	-5.3

Figure 6.2 shows an example of derived flus ratios for the entire FEPS sample and the positions of the calibration stars. As one can see, they are in the center of the locus of points define the position of the stellar photosphere. As all targets are observed in the SL1 and LL orders but not in the SL2 we opted to use two different sets of calibrators to ensure we used the best calibrators available. As the targets are observed at two different nod positions along the slit, and consequently are observed at two different positions at the detector array, two RSRFs need to be derived, one for each nod position separately. The resulting RSRFs are plotted in Figure 6.3 (black curves). Especially in the first orders differences between the nod positions can be seen, reflecting the differences in instrument characteristics between the two positions. The curves represent the mean of the selected targets per order as listed in Tables 6.2 and 6.3. We use a set of calibrators rather than a single star for the following reasons: 1) Improvement of SNR by combining observations and minimizing the possibility of propagating any spurious features due to effects like cosmic ray hits, and 2) Improvement of absolute flux calibration. Though we estimate the uncertainties of the reference Kurucz models to be only 3%, combining multiple observations should reduce this uncertainty by sqrt(N), under the assumption that no systematic effect exist.

The error on the RSRFs can be estimated by taking the standard error in the mean value. However, this error will consist of two parts: one part will reflect the noise in each observed spectrum and the other part will reflect the uncertainties in absolute flux calibration. In quoting errors for the RSRFs, this latter error should not be incorporated in the point to point error as it is irrelevant in the determination of error on spectral slopes or the significance of spectral features in each order. To separate the two errors, we use the following approach:

(1) Determine the mean RSRF from the entire dataset.

(2) Determine the RSRF for each calibrator separately.

(3) Multiply each dataset of individual calibrators with such factor that the individual RSRF correspond to the global mean RSRF.

(4) The standard error in the mean of the shifted dataset represent the point to point noise on the RSRF.

(5) The error in the mean of the factors calculated in step (3) represent the error in the absolute flux calibration of the RSRFs.

The error calculated in step (4) is plotted in Figure 6.2. We estimate the absolute flux calibration, as estimated following step (5), on the RSRFs to be 1%. This is in agreement with our estimate of the error on the Kurucz models of 3%, which should be reduced by a factor of 4 and 3 for the SL1 and LL orders, and SL2 order, respectively.

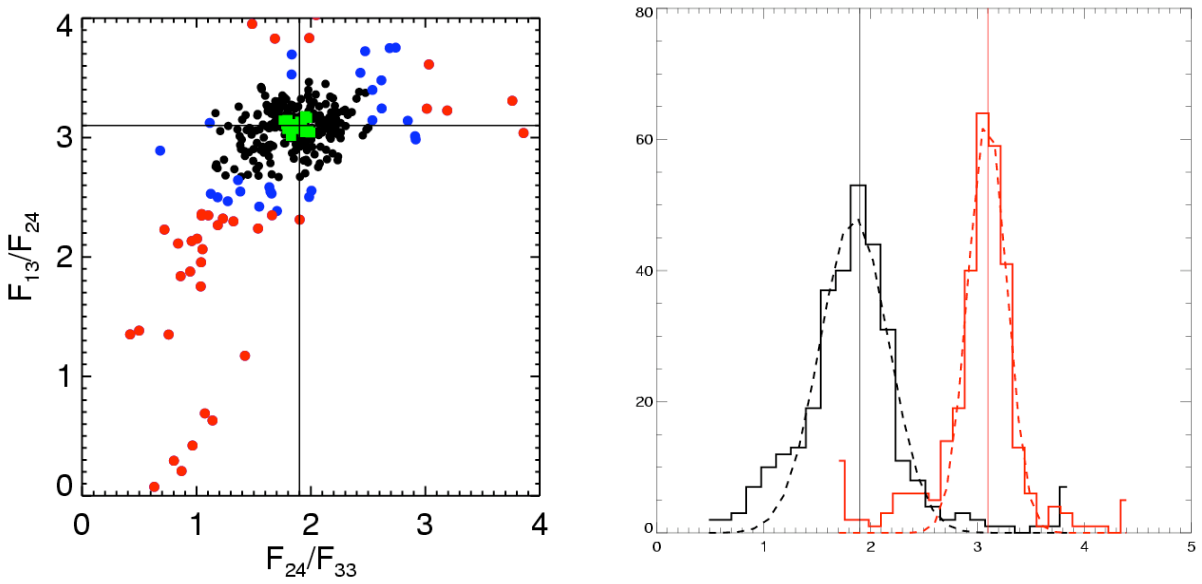

Figure 6.2 The distribution of color ratios for the entire FEPS sample. The left figure shows the flux ratio, based on synthetic photometry derived from the IRS spectra, at 13 micron over 24 micron, compared to the ratio of fluxes at 24 over 33 micron. The Red and blue symbols mark the positions of those systems having 3, respectively, 2 sigma deviating colors from the value of a stellar photosphere. This group consists of both excess sources and spurious observational results. The green symbols mark the position of the calibration stars as listed in Table 6.2. The right panel shows the histogram of the color ratios plotted in the left panel, together with a Gaussian fit (dashed line). The mean values (marked by vertical line) are in complete agreement with the expected values for a stellar photosphere.

Table 6.2: FEPS stars without an IR-excess used as IRS calibrators for the first order of the short-wavelength low-resolution module (SL1) and all orders of the long wavelength (LL) module.

NAME	SL1		LL	
	#cycles	Int. time	#cylces	Int. time
HD 92788	1	6	1	6
HD 88742	1	6	1	6
HD 28495	1	6	3	6
HD 209779	1	6	3	6
HD 190228	1	6	1	6
HD 90712	1	6	3	6
HD 193017	1	6	3	6
HD 106772	1	6	3	6
vB 52	1	6	2	14
HD 216275	1	6	1	6
HD 141937	1	6	3	6
HD 199598	1	6	1	6
HD 133295	1	6	3	6
HD 37006	1	6	3	6
HD 102071	1	6	3	6
HD 150554	1	6	3	6

We have checked if dependencies exist for the RSRFs on integration time and source brightness. In pipeline versions earlier than S11, such dependencies existed, due to incorrect droop and linearity corrections. We have found no evidence for such dependencies in the pipeline product used in this delivery. We therefore are confident that the derived RSRFs can be applied to observations using different integration time settings and to targets with different source

brightness. As a note, however, to this latter point, we stress that our RSRFs should only be applied to observations with similar or worse SNRs. Sources much brighter than our calibrators, especially at the longer wavelengths, most likely have much better SNRs, and applying our calibration could lead to the introduction of additional noise in the extracted spectra. As a second remark we would like to remind the reader that the derived RSRFs depend on the extraction aperture. If spectra are extracted using different apertures, each time a new set of RSRFs need to be derived, using identical extraction settings.

To summarize, these calibrations provide excellent order-to-order continuity, for targets of similar SNR as the FEPS target.

Table 6.3: FEPS stars without an IR-excess used as IRS calibrators for the second order of the short-wavelength low-resolution module (SL2).

Name	SL2 & SL3	
	#cycles	Int. time (sec)
HD 35850	1	14
AO Men	3	14
HD 174656	3	14
1RXS J105751.2-691402	3	14
HD 141521	3	14
HD 117524	6	14
1RXS J161318.0-221251	3	14
HD 284135	3	14
HD 146516	6	14
HD 120812	3	14

In the FEPS program, however, several T Tauri stars (TTS) with massive, optically thick disks have been observed. These stars, having a large excess, are substantially brighter in the infra-red than the other systems our program. Consequently, the SNR of the observations of the TTS is far better than the values typically found for the other targets , including the calibration stars listed in Tables 6.2 and 6.3. Applying the RSRFs (black curves) plotted in Figure 6.3 would therefore introduce noise in the TTS spectra, degrading their quality. To be able to correctly calibrate the spectra of the bright TTS stars, we selected the in Table 6.4 listed set of 6 bright calibrators, each observed at 6 different periods, provided by the SSC together with a Cohen stellar atmosphere model.

Table 6.4: IRS calibrators as provided by the SSC archive with Cohen stellar models, used to calibrate all orders of the short-wavelength low-resolution (SL) module and of the long wavelength low-resolution (LL) module.

NAME	AOR	SL1		SL2+SL3		LL1		LL2+LL3	
		#cycles	Int. time	#cycles	Int. time	#cylces	Int. time	#cycles	Int. time
HD 4138	8881920 8882688 9100800 9101568 9262592 9265664	1	6	1	6	2	120	1	120
HR 5467	9094912 9097984 10019328 10046976 13520896 13524480	1	14	1	14	2	120	1	120
HR 7018	8555520 8560896 11814144 11820544 12001536 12008704	1	14	1	14	2	120	1	120
HD 166780	9529344 9547264 12601600 12602880 13521408 13524992	1	6	1	6	4	30	1	30
HD 173511	8555776 8561152 9262848 9265920 10019584 10047232	1	6	1	6	3	30	1	30
HR 6348	9099520 9101056 13042176 13046784 13732352 13774336	1	6	1	6	4	30	1	30

Using the same procedure as described above we derived RSRFs based on the observations of the calibrators listed in Table 6.4 and their corresponding Cohen models. Though these RSRFs have a much better SNR, the absolute flux calibration, based on the entire FEPS sample is far superior. Therfore, we scale the RSRFs to our internal calibration. The results are plotted in Figure 6.3 (red curves). We used these latter curves to calibrate the FEPS observations delivered to the Spitzer data archieve.

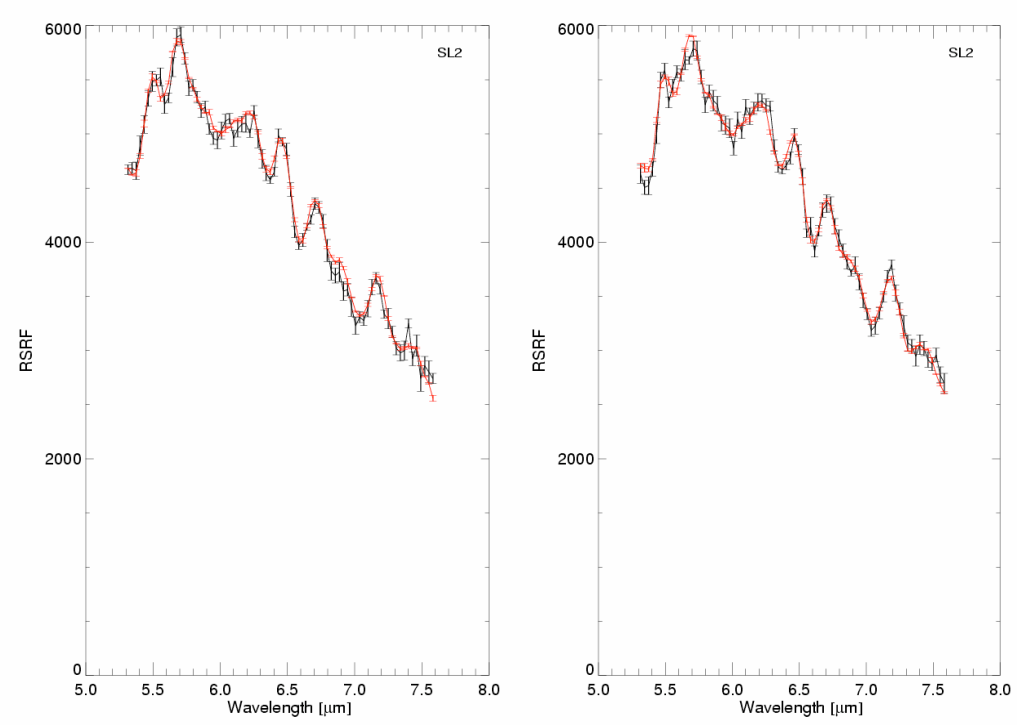

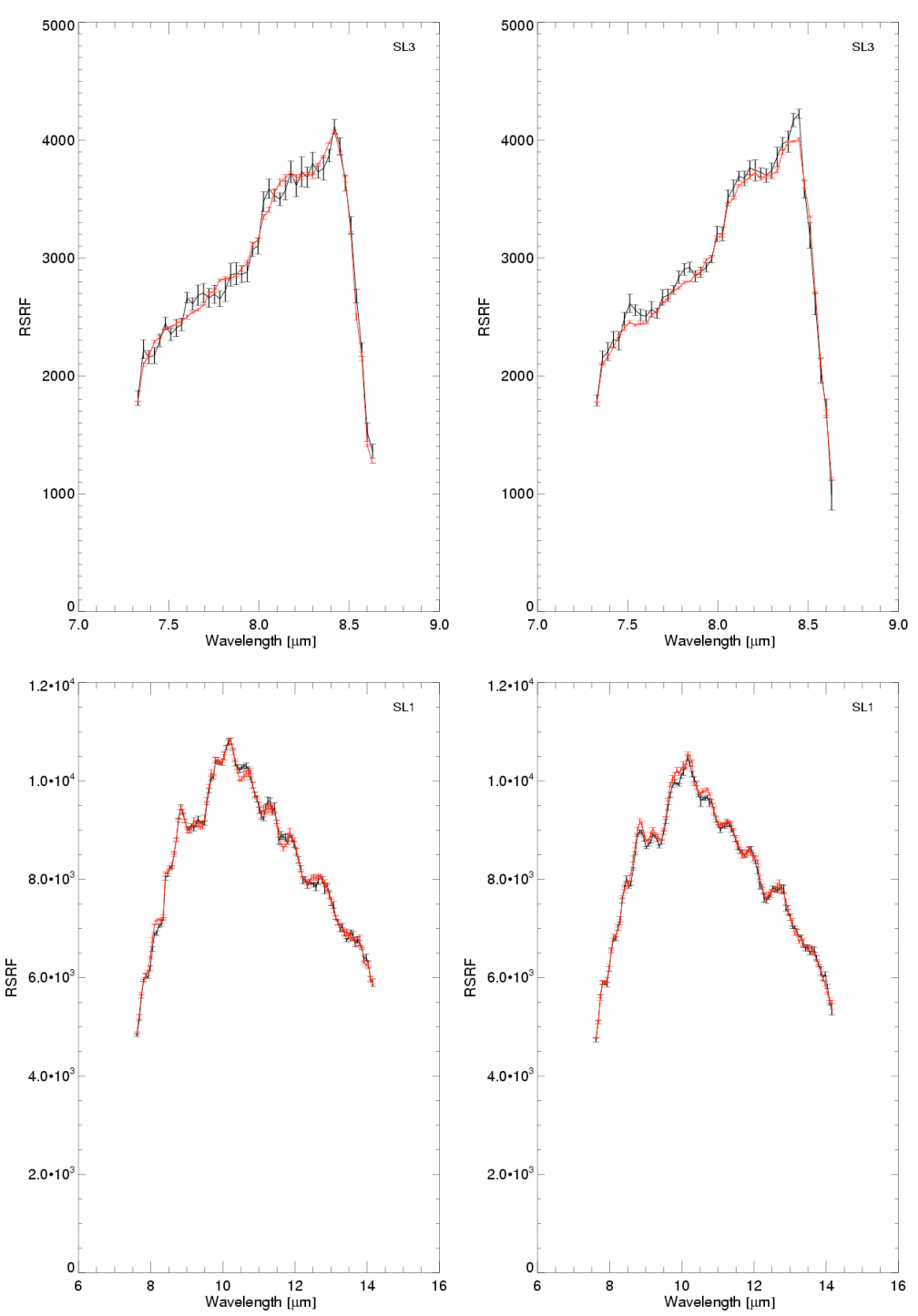

Figure 6.3: RSRFs derived from the FEPS target stars as listed in Tables 6.2 and 6.3 (black curves) compared to the scaled RSRFs derived from the calibrators listed in Table 6.4 (red curves). Plotted from top to bottom are the derive calibration for the SL2, SL3 and SL1, respectively. The left panels show the RSRFs derived for the 1/3 nominal slit position, the right panels for the 2/3 nominal slit position.

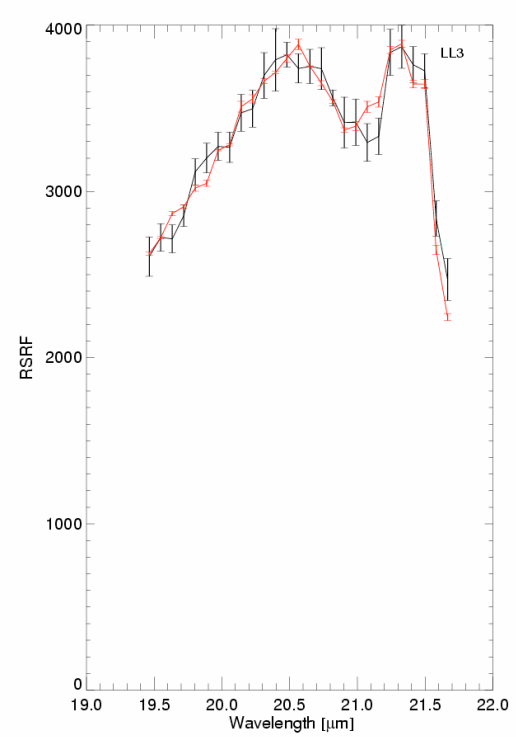
LL3
RSRF
Wavelength [μm]
0
1000
2000
3000
4000
19.0
19.5
20.0
20.5
21.0
21.5
22.0

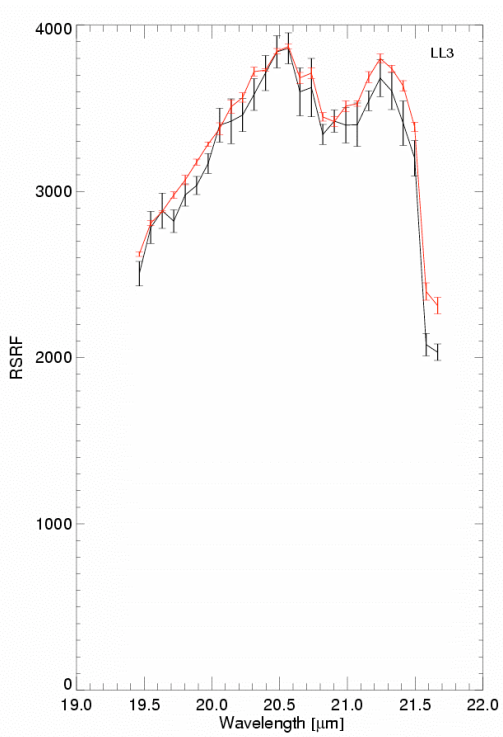
LL3
RSRF
Wavelength [μm]
0
1000
2000
3000
4000
19.0
19.5
20.0
20.5
21.0
21.5
22.0

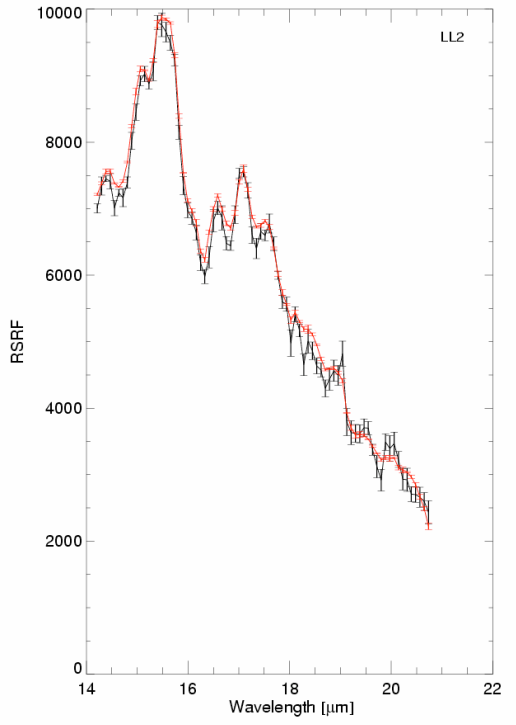
LL2
RSRF
Wavelength [μm]
0
2000
4000
6000
8000
10000
14
16
18
20
22

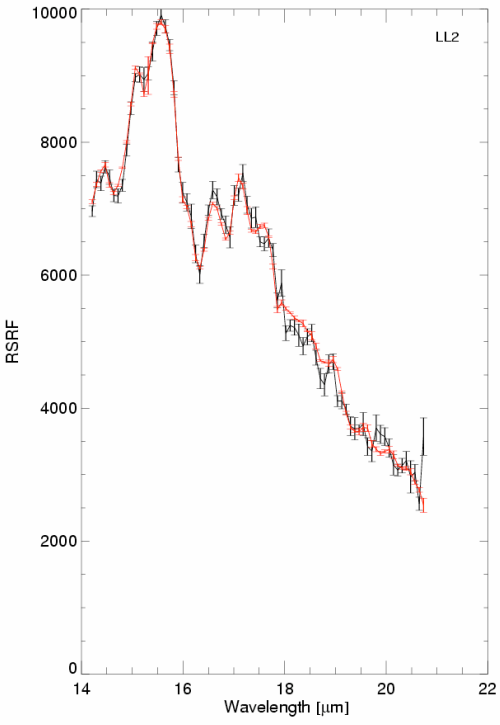
LL2
RSRF
Wavelength [μm]
0
2000
4000
6000
8000
10000
14
16
18
20
22

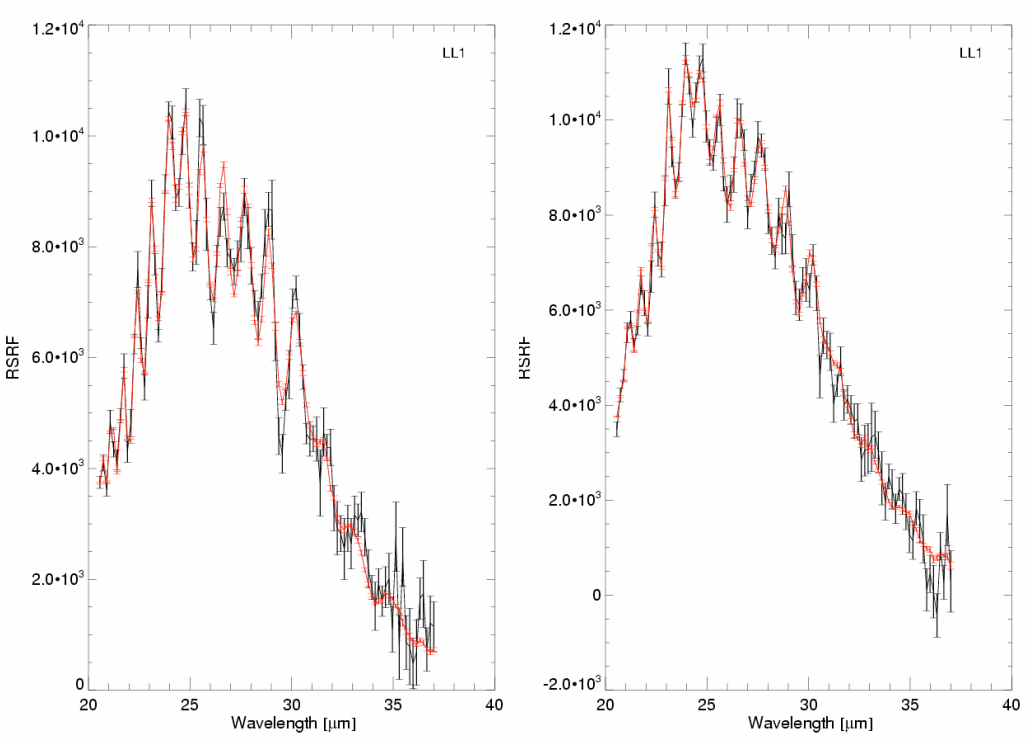

Figure 6.4: RSRFs derived from the FEPS target stars as listed in Tables 6.2 and 6.3 (black curves) compared to the scaled RSRFs derived from the calibrators listed in Table 6.4 (red curves). Plotted from top to bottom are the derive calibration for the LL2, LL3 and LL1, respectively. The left panels show the RSRFs derived for the 1/3 nominal slit position, the right panels for the 2/3 nominal slit position (see also Table 6.1).

6.2.3 Uncertainty Estimates

To be sure that the use of the standard deviation is meaningful, we have checked if the pixel noise in the spectral images is uncorrelated and has a Gaussian distribution. We used the observations of one of our FEPS target stars, 1RXS J155848.4-175758. This target star has 28 cycles for the LL module, which provides us with multiple values for individual pixels. We calculated for each pixel in the LL2 part of the background subtracted images, the difference between the measured pixel value Ipixel at position (x,y) and cycle j and the mean pixel value of multiple cycles <Ipixel>, divided by the sigma of the distribution at point (x,y):

$$D(x,y) = [Ipixel\_j(x,y) - \langle Ipixel \rangle(x,y)] / sigma(x,y)$$

The resulting distribution for the LL2 module for 28 cycles is plotted in Figure 5.6 with the solid line. Also plotted with the red dashed line is a fitted Gaussian, with a sigma of 1.07, indicating that the noise is indeed Gaussian.

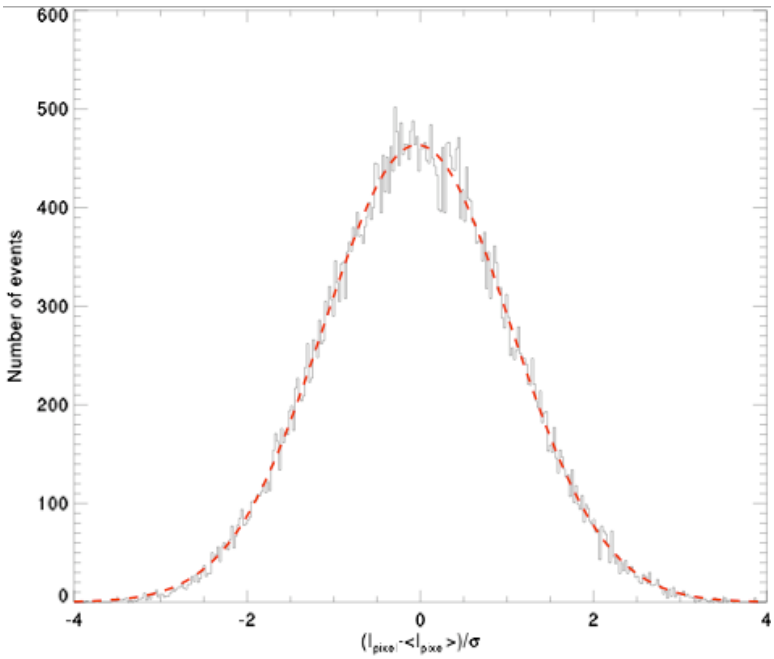

Figure 6.5 Uncertainty distribution of the pixel noise in the LL2 part of the spectral images of 1RXS J155848.4-175758. Also plotted is a Gaussian fit to the distribution (dashed red line) with a sigma of 1.07.

A slightly different way to demonstrate that the pixel noise is uncorrelated is shown by Fig. 6.7. Here the variance of the pixel values in the LL2 part (off-source observation) of the spectral images is plotted, using different numbers of cycles.

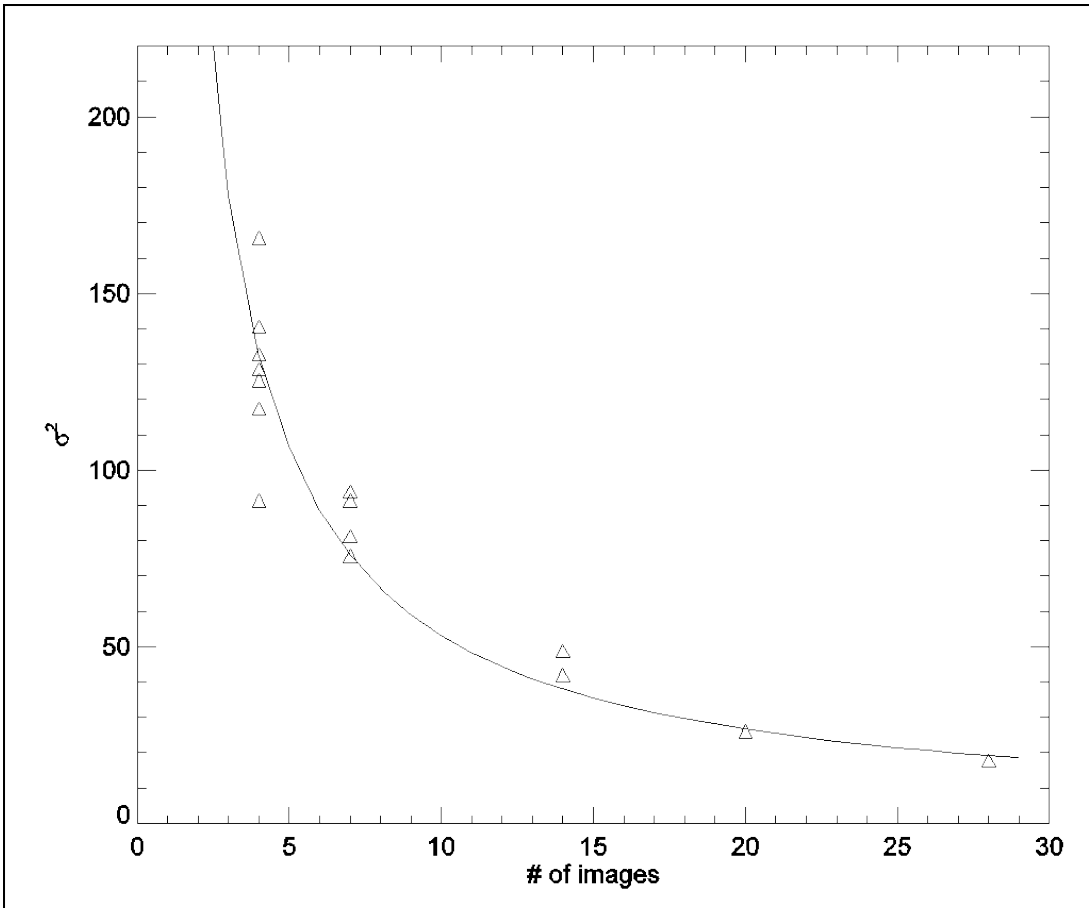

Figure 6.6 The behavior of the variance of the distribution of pixel values in the LL2 part of the spectral images of different numbers of used images (cycles). Also plotted with the solid line is a 1/number-of-images fit to the calculated variances.

If the pixel noise in each cycle has a Gaussian distribution, the variance should have a 1/N behavior, with N the number of images (cycles) used to calculated the variance. Indeed this behavior can be observed as is demonstrated by the 1/N fit to the data points shown in Fig. 6.7 (solid line). This means that one can use the mean spectral value over cycles and slit positions to calculate the mean spectral value, and the standard deviation in the mean of the distribution of data points as a meaningful estimate of the uncertainty in the measured fluxes.

Given the above discussion, the fluxes values and errors provided to the SSC archive by the FEPs legacy team are divined by the following. For the flux calibration, we derived the RSRFs by using the observations of the set of calibrators as listed in Tables 6.3 and 6.3, and their stellar models (see previous section for details). The estimated standard error on the RSRFs, is incorporated into the final calibrated spectra. The difficulty is that the RSRF has to be applied for both nods separately, but that the error estimate of the spectra is an average including both nod positions, which cannot be determined before applying the calibration. We estimate therefore the final error by estimating a average error on the RSRF by taking the RMS and combining this with the error on the extracted spectra. The calibrated spectra and error are thus defined in the following way:

$$F(\lambda) = \sum_j \left(\sum_i \left(F_{droop}(\lambda)_i / RSRF_i \right) \right) / N$$

$$\frac{\Delta F(\lambda)}{F(\lambda)} = \sqrt{\left[\left(\frac{\Delta F}{F} \right)^2 + \left(\left(\frac{\Delta RSRF_1}{RSRF} \right)^2 + \left(\frac{\Delta RSRF_1}{RSRF} \right)^2 \right) / 2 \right]}$$

where *j* is the number of cycles, *i* the nod position (1 or 2).

6.2.4 Order Stitching

For each target a combined one-dimensional spectrum is delivered. The orders are stitched together by taking the mean flux at overlapping wavelength points, no wavelength shifting or spectral tilting of any sort is performed. The error quoted in these per wavelength element N overlapping data points is calculated as follows:

$$F(\lambda) = (1/N) * \sum [F_i(\lambda)]$$

$$\Delta F = \sqrt{ \sum_i \left[\left((1/N) * \sigma_i \right)^2 \right] }.$$

The last column in the delivered spectral tables indicates to which module the data point belongs. These are bit values where the 0,1,2,3,4,5 bit is set for the SL1, SL2, SL3, LL1, LL2, LL3 module respectively in overlapping wavelength points. Observations using the Infrared Spectrograph (IRS) low resolution modules (R~64-128) from 7.4 –38μm will be obtained for all objects of the FEPS sample[5]. Observations using the Short-Lo 1 (SL1) module (5.2 – 7.4μm) were obtained for the first five validation targets and for all stars with ages in the range of 3-30 Myrs. Dropping the SL2 observations for the older stars was deemed acceptable for older objects because no spectral features other than from the stellar photosphere are expected over this wavelength region. The time saved by not using the SL2 for all targets allowed for longer integration times for instrument modes that were found to be underperforming compared with pre-launch estimates.

6.3 IRS High Resolution Spectra

We release high-resolution spectra, line fluxes and upper limits for 19 FEPS sources belonging to our gas survey (see Table 6.5). This sample includes all sources up to the IRS campaign 22 included except HD 105, which has a much lower quality spectrum because it was acquired without sky exposures. The data reduction required additional care in estimating the proper background. This dataset and line fluxes are published in Hollenbach et al. (2005).

The deliver objects have been all observed in the same cluster-offset mode with two nod positions on-source and two additional sky measurements. Near-simultaneous sky observations

[5] A few stars will be observed as part of other science programs. This data will be analyzed by the FEPS team and incorporated into our released products when the proprietary period on the observations has expired.

are used to properly subtract the sky background and to mitigate the effects of anomalous pixels, especially prominent in the LH module. The IRS or PCRS Peak-up options were used to carefully position the sources in the slit.

The spectra of the first 8 targets in Table XX were already included in the previous data release. We re-processed all the data uniformly and used additional bad pixel masks from the SSC which were not available for the previous release. This approach resulted in cleaner spectra with typically a factor of two improvement in the line flux upper limits.

Table 6.5: Summary of delivered spectra

Source	SH	LH	Peak-up
	Seconds X ncycles	Seconds X ncycles	
HD 134319	31.46 X 6	14.68 X 10	IRS blue moderate
HD 143006	6.29 X 8	14.68 X 8	PCRS
HD 17925	31.46 X 5	14.68 X 8	IRS red moderate
HD 202917	31.46 X 5	14.68 X 8	IRS blue moderate
HD 216803	31.46 X 5	14.68 X 8	IRS red moderate
HD 25457	6.29 X 4	6.29 X 2	IRS red moderate
HD 35850	31.46 X 6	14.68 X 10	IRS red moderate
HD 37484	31.46 X 10	14.68 X 10	IRS red moderate
1RXS J162948.8-215205	121.9 X 6	60.95 X 8	IRS red moderate
1RXS J122233.4-533347	121.9 X 6	60.95 X 6	IRS blue moderate
1RXS J130153.7-530446	121.9 X 6	60.95 X 7	IRS blue moderate
1RXS J132207.2-693812	6.29 X 3	14.68 X 2	PCRS
AO Men	121.9 X 2	60.95 X 2	IRS blue moderate
HD 119269	121.9 X 2	60.95 X 3	IRS blue moderate
HD 12039	121.9 X 4	60.95 X 3	IRS blue moderate
HD 209253	31.46 X 7	14.68 X 4	IRS red moderate
HD_377	121.9 X 3	60.95 X 3	IRS blue moderate
RX_J1111.7-7620	31.46 X 7	60.95 X 8	PCRS
V343NOR	121.9 X 2	60.95 X 2	PCRS

6.3.1 Data Reduction of the Sources with Associated Sky Observation

Raw IRS data are first processed on a DCE basis with the SSC pipeline S12.0.2. We start our data reduction from the so-called {\it droop} products. Corrections applied in the SSC pipeline at this stage include: saturation flagging, dark subtraction, linearity correction, cosmic ray rejection and integration ramp fitting.

The data reduction is based on self-developed IDL routines in combination with the SMART reduction package developed by the IRS Instrument Team at Cornell (Higdon et al. 2004). The first step of the data reduction consists in creating background-subtracted images from sky measurements of the same nod position as the on-source exposures.

Next the dead, bad and hot pixels are corrected using the IRSCLEAN package built in a joint effort by the Cornell IRS Instrument Team and the IRS Instrument Support Team at the Spitzer Science Center. The cleaning occurs by: a) averaging spatial profiles in rows above and below the affected row; b) normalizing the average profile to the affected row; c) replacing the flagged pixel with the pixel from the averaged profile.

We fix pixels marked bad in the "bmask" files with flag value equal to 2^9 or larger, thus including the permanently bad pixels masked in the "pmask". The SSC provides additional hot pixel masks for individual campaigns/modules.

In this data release we also correct for these hot pixels. The routines recognize if a pixel is marked in both the dmasks and the additional hot pixel masks and correct only once. We are investigating on-the-fly identification methods for hot pixels that we will apply in the next data delivery.

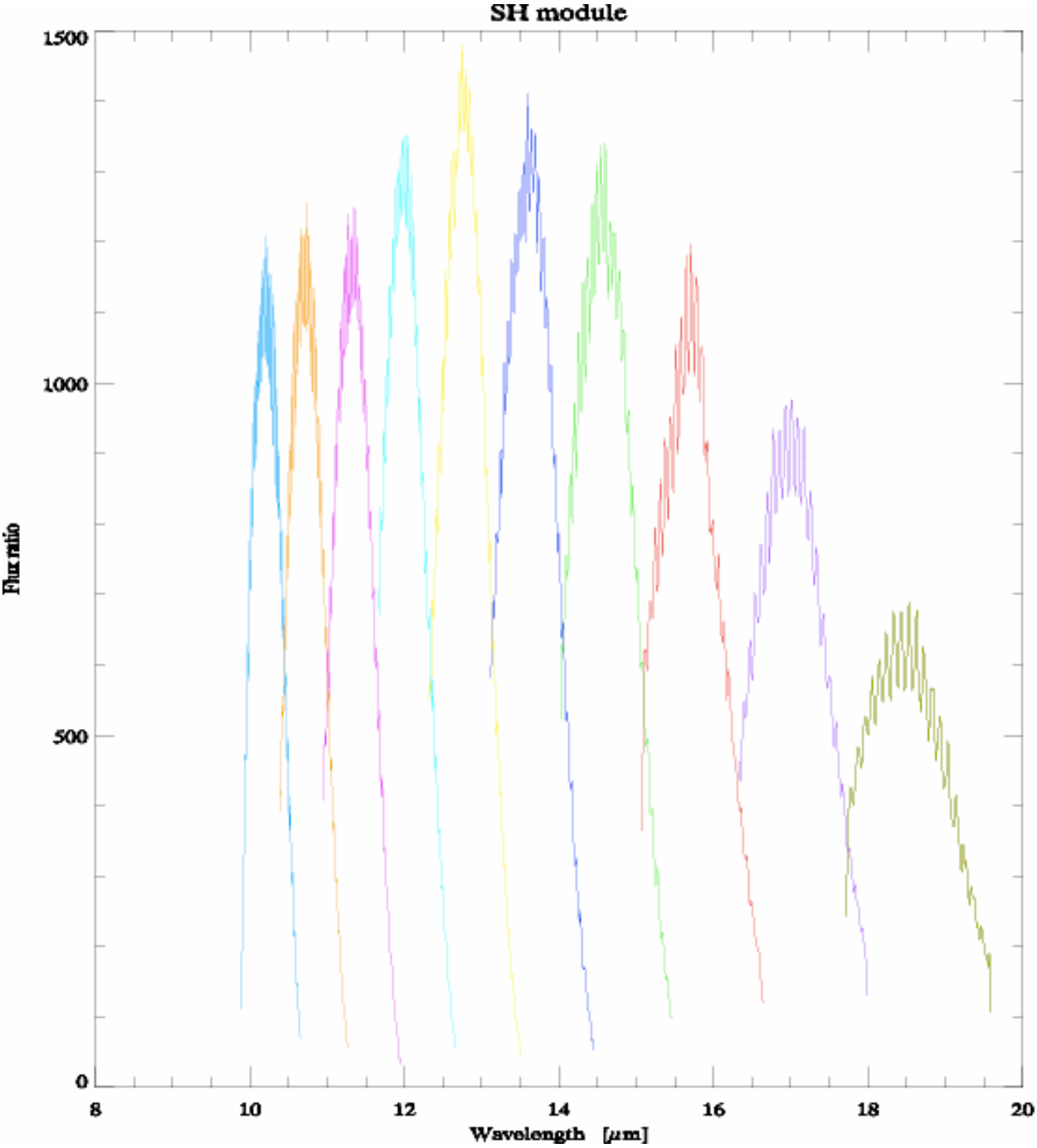

Figure 6.8: RSRF for the SH module. Different colors represent different orders.

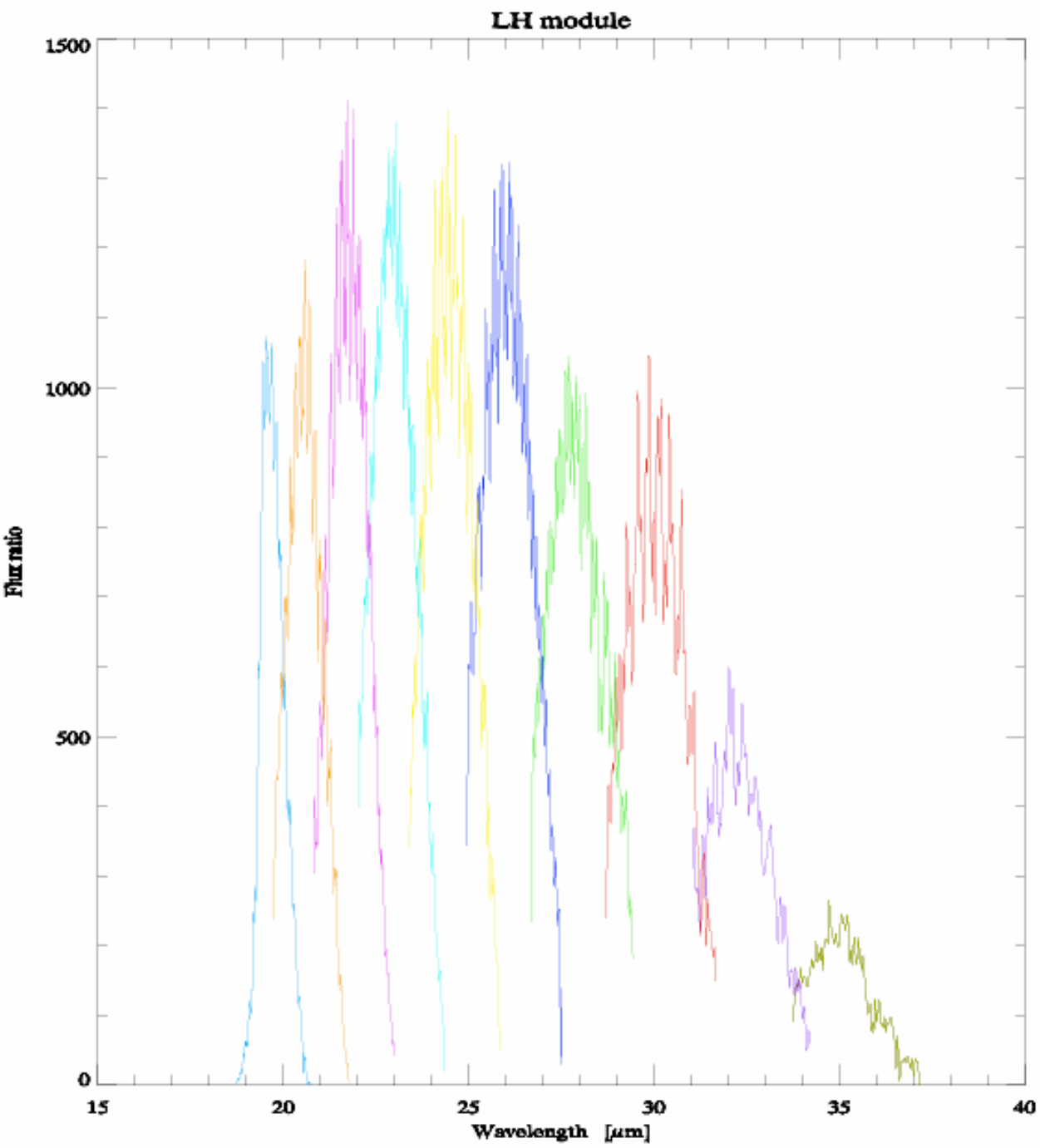

Figure 6.9: RSRF for the LH module. Different colors represent different orders.

We then use the background pixel-corrected images to extract 1D spectra with the full aperture extraction routine in SMART. The same procedure is applied to our sources and to calibrators observed in the Spitzer IRS Calibration program (PI, L. Armus). We used all the calibrators processed with the S12 pipeline (2 observations of HD 166780, 3 of HD 173511 and 1 of Ksi Dra) to create two one-dimensional spectral response functions (one at each nod position) from the known stellar model atmosphere (see Figures 6.8 and 6.9). The stellar models for the

calibrators are available at the SSC web page[6]. The extracted spectra of each source are then divided by the spectral response function on an order and nod basis.

The low right side of the chip is not well illuminated resulting in a drop of signal at the end of each order. However, since the orders have a good overlap in wavelengths, we trimmed the low-signal regions: the overlapping regions are about 0.06 μm in the SH module and 0.1μm in the LH module.

After trimming, spectra over all slit positions and cycles are averaged on an order basis. The errors at each wavelength are the 1σ standard error of the distribution of the data points used to calculate the mean spectrum over all cycles and nod positions. The error or the calibration is included in similar manner to the low-resolution spectra. After that, the orders are stitched together by taking the mean flux at overlapping wavelength points, no wavelength shifting or spectral tilting of any sort is performed. The error quoted at overlapping wavelengths is the error propagation of the mean value:

$$\text{error}(F\_\text{mean}) = \text{sqrt}(\text{sum\_i}((1/N*\text{sigma\_i})^2))$$

The last column in the delivered spectral tables indicates to which order(s) the data point belongs. In the overlapping wavelengths both order numbers are present: For example, the last column of the table at the wavelength 10.456μm is 2019.

6.3.2 Line Fluxes and Upper limits

The IRS SH and LH modules cover several atomic and molecular lines (see e.g. linelists posted at http://www.ipac.caltech.edu/tools/ , most of which are expected to be unresolved at the IRS resolution. Our gas and dust modeling of representative targets from our sample predicts seven strong transitions from circumstellar disks (Gorti & Hollenbach 2004, Hollenbach et al. 2005). Therefore, in addition to the high-resolution spectra we provide for each object the fluxes (detection) or upper limits (non-detection) of the seven transitions.

To estimate line flux upper limits, we first fit the spectrum with a first order polynomial using a Levenberg-Marquardt (LM) algorithm implemented in custom IDL routines. The fitting is performed in the wavelength range of 1 micron centered on the expected feature. Five-sigma upper limits to the line fluxes are computed from the local RMS dispersion in the continuum and the resolution element at the specific wavelength. In the case of detection, we fit a Gaussian to the line with the width matched to the instrumental line profile and provide the line flux.

[6] http://ssc.spitzer.caltech.edu/irs/calib/templ/.

This information is summarized in an additional table that accompany each spectrum. The table is structured as follows:

- Column (1) – wavelength of the transition in micron
- Column (2) – RMS of the continuum in Jy
- Column (3) – line flux or five sigma upper limit in W/cm^2
- Column (4) – line identification and comments.

6.3.3 Caveats (Needs Revision)

6.3.3.1 Artifacts

Narrow spikes in the spectra can be often associated with anomalous pixels which have not been flagged in the SSC masks and therefore not corrected by our current version of the pipeline. We note that such spikes are mainly present in the LH module, the background subtraction in the SH module effectively remove most of these outliers.

Artifacts at the edge of the orders can be due to non adequate flat-fielding of the BCD products and/or bad order matching. We tested that these artifacts can be greatly reduced by using "droops" products and applying a 1 dimensional spectral response function obtained from calibrators available from the SSC extracted exactly in the same way as our targets. We are currently working on an improving our spectral response function and plan to apply the described data reduction procedure in the next data delivery.

6.3.3.2 Calibration

We compared all the delivered high-resolution spectra with our IRS low-resolution spectra and, when available, infrared photometry from the literature. For all the sources but the young HD 143006, the agreement between the high-resolution and low-resolution spectra is within the quoted error bars (<10%). In the case of HD 143006, we note that there is a discontinuity of about 14% between the SH and LH module, with the SH module well in agreement with the low-resolution spectra. This discontinuity reduced when using a 1 dimensional spectral response function on spectra extracted from droops data.

6.3.3.3 Defringing

Fringes observed in the IRS spectra have usually amplitudes of ~1 to 3% depending on the order and wavelength. Since the noise in most of our spectra is high, due to the artifacts discussed above, and overwhelms the few % fringes, we did not use the IRSFRINGE package to defringe the delivered spectra.

7 Multiband Imaging Photometer for Spitzer (MIPS) Data

MIPS provides photometric imaging in three bands centered at approximately 24, 70 and 160μm. All of the FEPS targets used the photometric imaging mode, which yields multiple pointings at the target with small offsets between each pointing. This strategy alleviates many of the instrumental artifacts and cosmic rays that are not otherwise removed by the pipeline processing. In addition, due to the stable sensitivity of the Si:As array, these multiple pointings for the 24μm data, allow the repeatability of the observations to be used as an accurate estimate of the photometric uncertainties.

7.1 MIPS Data and DAT pipeline

The MIPS data for FEPS was reduced using the Data Analysis Tool developed by the MIPS Instrument Team at the University of Arizona (Gordon et al. 2004). This package uses the raw data product available from the SSC data archive, and does not rely on any other SSC processing. The SSC pipeline products may be used in future releases of the FEPS MIPS products once the SSC pipeline have reached the same level of maturity as the DAT.

7.1.1 The Si:As 24μm Data

For 24μm observations we use default scales, small field size, and 3 and 10 second exposure time per Data Collection Event (DCE). In general, FEPS observations use NCYCLES = 2 cycles, and produce 28 DCEs[7]. Fainter objects requiring longer integration used multiple cycles, resulting in N*16 images per target.

The dark subtraction, scan mirror dependent flat field, electronic nonlinearity correction, droop subtraction, and cosmic ray rejection were applied using the DAT. The scan-mirror-dependent flat fields are necessary to remove flat field features that are caused by debris on the MIPS pick-off mirror; these features "move" relative to the sky as the scan-mirror is moved.

7.1.2 The Ge:Ga 70μm and 160μm Data

For the 70μm and 160μm Ge:Ga array data, FEPS uses default scales, small field size, and 10 sec exposure time per DCE. NCYCLES vary depending on targets, 2 - 14 cycles for 70μm. Photometry mode produces a minimum of 8 images of the object at 70μm per cycle. Again, increasing integration time generates integer multiples of this number of images.

The FEPS V2.0 release contains MIPS 160μm observations of 36 stars. FEPS uses the default scale, small field size, with 10 sec exposure except for one source (HD 143006) that we used 3 sec exposure time. We use 2 or 4 cycles for all 160μm observations; 4 cycles at 160μm approaches the MIPS-measured confusion limit (Dole et al. 2004). A typical final 160μm mosaic image contains 16 DCE coadded frames.

[7] One DCE corresponds to one image.

7.2 MIPS Point-Source Photometry

For all 24, 70, and 160μm data, photometry was performed on mosaic images produced by the enhancer portion of DAT pipeline (Gordon et al. 2004); the final mosaic images are free of primary instrument artifacts. All images were visually inspected to identify confusing sources and to check for obviously resolved systems. Inspection of the MIPS images shows that the FEPS stars are unresolved, allow use simple aperture photometry.

All photometry and image analysis for 24μm data and most of the 70μm data were performed using IRAF (version 2.12.2a). For about seventy 70μm sources that needed more careful photometry due to nearby sources or complicated background, we used IDP3 (Schneider & Stobie 2002)[8]. All photometry and analysis for 160μm data were performed using IDP3.

The position of the aperture was found by fitting a two-dimensional Gaussian to the core of the PSF. The aperture photometry was then performed on the target centered at the fit position. The aperture radius, background annulus, and aperture correction values are given in Tables 7.1 and 7.2.

For 24μm data, an aperture radius of 6 pixels and background annulus of 12 to 17 pixels were used for most of the stars. Aperture radius of 3 pixel was used for most of the cluster stars (e.g., Pleiades stars), faint sources, and for the sources with neighboring sources that contaminates stellar fluxes if using 6 pixel radius.

For 70μm data, default aperture radius used was 3 pixels with background annulus of 4 to 8 pixels. For sources that have contaminating nearby sources in background annulus by about 5%, we masked out the neighboring source(s), and used aperture radius of 2 pixels with the same background annulus size. These 70μm fluxes done on masked images are indicated in the flag column of the flux table of FEPS sources in this version of data delivery. For all 160μm data we use a default target aperture radius (3 pixels) and background annulus size (3 to 5 pixels) (see Table 7.1).

Table 7.1 shows the adopted aperture radii and background annuli for MIPS photometry. Table 7.2 shows the associated aperture corrections and the fraction of the PSF flux that is contained within the background annulus. Aperture correction factors were derived using STinyTim PSF images available from the SSC website. PSF images were scaled to have the same pixel size for each mosaic images before deriving the aperture correction factors.

Flux Density (corrected) = (measured flux density)/(aperture correction factor)

[8] IDP3 was developed by the Instrument Definition Team for the Near Infrared Camera and Multi-object Spectrometer to do aperture photometry.

Table 7.1: MIPS aperture sizes, background radii, and aperture corrections photometry.

Wavelength (μm)	Target Radius (pix)	Background Inner Radius (pix)	Background Outer Radius (pix)
24	3,6	12	17
70	2,3	4	8
160	3	3	5

Table 7.2: MIPS Aperture corrections and fraction of PSF contained in Background Annulus

Wavelength (μm)	Apcorr
24	0.63498, 0.87719
70	0.57962, 0.76541
160	0.52628

7.3 Photometric Calibration, Wavelengths and Color Corrections

The (1σ) absolute photometric calibration of MIPS is currently 10%, 20% and 20% for 24, 70 and 160μm respectively. The delivered products include only the internal (precision) uncertainties, so comparison of the FEPS photometry should take into account the additional calibration uncertainties listed above. We note that the MIPS calibration is tied to the "weighted average" wavelengths of each filter/detector combination (23.68μm, 71.42μm, 155.9μm). The photometry reported in the FEPS data products do not have a color-correction applied. For a 10,000 Kelvin black-body, the color-correction is 1.000. Users are cautioned that a color correction should be applied based on the tables available from the SSC.

7.4 MIPS Mosaic Images

For all three MIPS bands, images were combined using the Enhancer subroutines of MIPS DAT pipeline (Gordon et al. 2004, 2005 for details). The files are multi-extension FITS files:

- plane 1: surface flux density (in μJy/sq. arcsec)
- plane 2: uncertainty in surface flux density
- plane 3: data flag
- plane 4: total number of sky sightings used for coadding.

The co-adding takes place in a tangent plane to the average right ascension and declination of images. Before the individual DCEs are coadded, the pixel locations for each DCE image are corrected for optical distortion.

The Enhancer has options for producing "super-resolved" images by building the mosaic image on a sub-pixel grid with pixel scale smaller than the native instrument pixels. However, we have opted to construct the delivered mosaic images using the native pixel scale, namely subpixel scaling of 1. To mitigate poorly corrected bad pixels and residual cosmic ray signals, an outlier rejection has been performed for each subpixel in the mosaic image where multiple sightings of the sky exist. The number of co-added sky sightings per pixel is recorded in the fourth plane of the final mosaic image.

Table 6.3 lists the final (rectified) pixel scales and flux conversion factors for the final mosaiced images are below:

Table 7.3: Rectified pixel scale for mosaiced MIPS images.

MIPS Band	(sub-) pixel size(")	flux conversion factor
24μm	2.49	1.032 [μJy/arcsec^2/(DN/s)]
70μm	9.85	1.49x10^4 [μJy/arcsec^2/mips_70_unit]
160μm	16.00	1000 [μJy/arcsec^2/mips_160_unit]

7.4.1 24μm Mosaics

Scan mirror dependent flat field files were used for all DCE images. We created an "on the fly" 24μm flat field images that uses a master flat field image that is shifted to match the spot pattern for individual 24μm images. The final mosaic images were made using the MIPS DAT.

7.4.2 70μm & 160μm Mosaics

The 70μm and 160μm were made using the MIPS DAT. However, for the 70μm images reduction process, a median value of the columns is taken out from each column in each DCE image to mitigate the residual column to column offsets. Then we apply a "time-filter" that is a simple boxcar filter where the average value (after interactive sigma rejection) of the values of a pixel for a window centered on the current DCE is subtracted from the current DCE. To prevent the current DCE from biasing the result, the current DCE and the DCEs immediately before and after are excluded from the filter. The window is set to empirically maximize the signal-to-noise with a width of 35 DCEs.

No time filtering has been applied to the 160μm data at this time. Electronic non-linearity for 70μm and 160μm is now corrected.

8 Ensemble Characteristics of the FEPS V3.0 Data Release

The FEPS V3.0 data release contains IRAC & MIPS photometry plus IRS low resolution spectra for 291 stars. This large dataset allows us to evaluate the characteristics of the ensemble, and in particular, the achieved precision and accuracy of the IRAC and MIPS photometry. In addition, we can consider the cross calibration between the IRAC, IRS and MIPS.

8.1 IRAC & MIPS Photometry

We first consider the aperture photometry from the IRAC and MIPS images. An estimate of the internal uncertainty for each measurement is outlined for IRAC (Section 4) and MIPS (Section 6). Here we re-evaluate these uncertainties based upon the behavior of the characteristics of the ensemble of the data. The internal uncertainty (i.e. precision) is derived empirically from the RMS scatter of the Spitzer colors, and the calibration uncertainties (i.e. accuracy) are evaluated with respect to Kurucz model atmospheres. A summary of the minimum internal uncertainties for the IRAC channels and MIPS 24μm, expressed as percent uncertainty in the flux, is provided in Table 8.1a. Analysis of the MIPS 70μm and MIPS 160μm photometry suggests that the internal uncertainties in the MIPS 70μm uncertainty, as reported in the FEPS database, are underestimated by a factor of 3.3.

The calibration uncertainties were assessed by comparing the observed photometry with the model fluxes computed from the best-fit Kurucz model atmospheres. Table 8.1b indicates the multiplicative factors that should be applied to the IRAC and MIPS 24μm fluxes in order to place the observed fluxes on the same calibration scale of the Kurucz models. One must consider two important caveats before applying these calibration factors to actual data: 1) the Kurucz models themselves may (likely) have systematic errors relative to actual stellar photospheres, and 2) these calibration factors are the mean values derived from the data, as there are systematic trends as a function of magnitude that are as large as a 3.8%. In generating the photometry summary for the SSC, the minimum flux uncertainties in Table 1a have been applied (as well as the ad hoc increase in the MIPS 70μm and MIPS 160μm internal uncertainties), but the calibration factors in Table 8.1b have not.

Table 1a. Adopted Minimum Internal Uncertainties

Band	Uncertainty (percent)	Comments
IRAC 3.6um	0.85	
IRAC 4.5um	0.85	
IRAC 5.8um	1.4	
IRAC 8.0um	1.7	
MIPS 24um	6.0	for [4.5] < 7.0 mag
MIPS 24um	17.6	for [4.5] > 7.0 mag

Table 1b. Mean Calibration Factors

Band	Factor	Comments
IRAC 3.6um	0.92	
IRAC 4.5um	0.95	
IRAC 5.8um	0.91	
IRAC 8.0um	0.93	
MIPS 24um	0.99	for [24] < 7.0 mag
MIPS 24um	0.94	for [24] > 7.0 mag

8.1.1 Internal uncertainties in the IRAC photometry

The IRAC data were obtained in subarray mode, and a dataset for each star consists of 4 dither positions of 64 frames each for a total of 256 frames. Photometry has been measured on each frame individually, and the internal IRAC photometric uncertainties have been estimated by computing the standard deviation of the mean of the 256 measurements. Formally, the internal IRAC uncertainties are less than 1% for all but one star at 3.6μm and 4.5μm, and 17 stars at 8.0μm. However, the standard deviation of the mean will underestimate the photometry uncertainties since there may be systematics that limit the photometric precision of the observations. In this section, I estimate the minimum uncertainties in the IRAC photometry based on the observed dispersion of the IRAC colors.

To empirically estimate the photometric uncertainties, we computed the RMS scatter in the IRAC colors for the stars in this data release. The assumption is that since the visual extinction is generally a few magnitudes or less for the FEPS targets, and most of the sources do not appear to exhibit an infrared excess in the IRAC bands, then the dispersion in the IRAC colors reflects primarily the internal photometric uncertainties.

Figure 8.1 presents scatter plots (left panels) of IRAC colors vs. IRAC magnitudes, and histograms (right panels) of the colors. Five sources have an infrared excess in the IRAC bands and are mainly offscale on these plots. Table 2 below presents various statistics on the mean and rms of the IRAC colors after excluding the 5 IRAC excess sources. Statistics are computed over all magnitudes as well as separately for stars brighter than and fainter than 7.0 magnitude.

These results show that the dispersion in the [3.6]-[4.5] color is 0.012 mag, 0.020 to 0.021 mag for [4.5]-[8.0], and 0.017 to 0.019 for [3.6]-[8.0]. Careful inspection of Figure 1 also shows that there is a trend in the [3.6]-[8.0] and [4.5]-[8.0] colors as a function of magnitude such that sources brighter than 7.0 mag are bluer by 0.008-0.014 mag compared to fainter sources. Even after splitting the sources into two brightness intervals (i.e. brighter and fainter than 7.0 magnitude), the RMS dispersion in the colors is ~ 0.02 mag. Therefore, the higher dispersion in the [3.6]-[8.0] and [4.5]-[8.0] colors cannot be attributed to the trend of the color with magnitude.

From Table 8.2, we adopt 0.012 magnitude as the dispersion in the [3.6]-[4.5] color. Assuming that the internal uncertainties in the [3.6] and [4.5] magnitudes are the same, then the implied uncertainty in the magnitudes is 0.012 / sqrt(2) = 0.009 mag. The corresponding uncertainty in the flux is then ln(10) / 2.5 * 0.010 = 0.83%. We therefore adopt 0.83% as the minimum flux uncertainty in the IRAC 3.6μm and IRAC 4.5um bands. If the standard deviation of the mean of the 256 measures for a given star is larger than 0.83%, the standard deviation of the mean is adopted as the flux uncertainty.

Similarly, for the [4.5]-[5.8] color, the RMS dispersion is 0.014 mag (although based on only 5 stars). Given the adopted uncertainty of 0.009 mag for [4.5], the implied uncertainty in the [5.8] magnitude is 0.011 mag, or 0.99%. For the [3.6]-[8.0] color, the RMS dispersion is 0.022 mag. Given the adopted uncertainty of 0.009 mag in [3.6], the implied uncertainty in the [8.0] magnitude is 0.020 mag = 1.8%. We therefore adopt 0.99% and 1.8% as the minimum uncertainty for the IRAC 5.8μm and IRAC 8.0μm photometry.

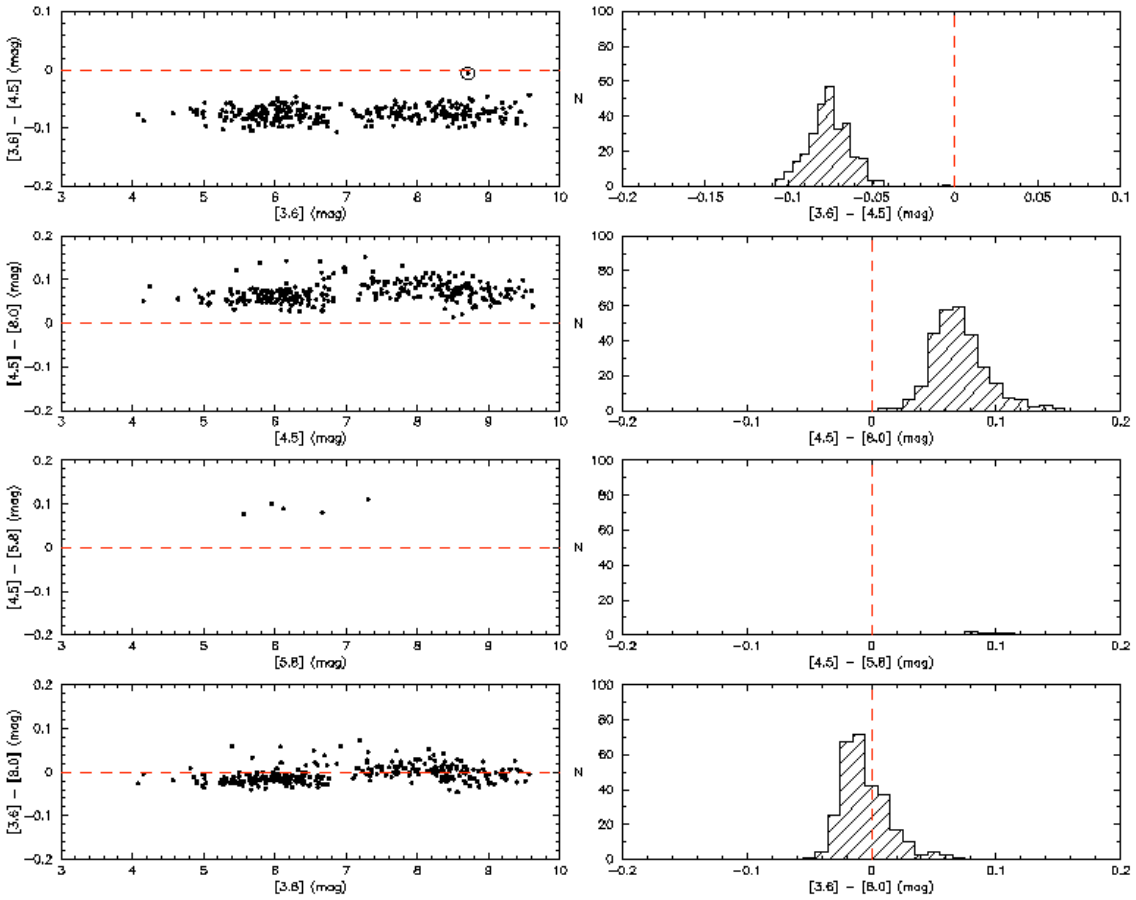

Figure 8.1: Plot of the observed IRAC colors vs. magnitude (left panels) for stars in the V3.0 data release, and histograms of the IRAC colors (right panels). Five sources have infrared excesses above the stellar photosphere in the IRAC bands; these excess sources are represented by open circles, but most are located offscale on these plots. The dashed line at color=0.0 is shown for reference.

Table 8.2: Measured IRAC Colors for FEPS V3.0

Color	Magnitude Range	Mean (mag)	RMS (mag)	Nstars
[3.6]-[4.5]	All	-0.076	0.012	286
	[3.6] < 7.0	-0.077	0.012	147
	[3.6] > 7.0	-0.074	0.012	139
[3.6]-[8.0]	All	-0.006	0.019	286
	[3.6] < 7.0	-0.012	0.017	147
	[3.6] > 7.0	0.002	0.019	139
[4.5]-[5.8]	All	0.092	0.014	5
[4.5]-[8.0]	All	0.070	0.022	286
	[4.5] < 7.0	0.064	0.020	147
	[4.5] > 7.0	0.076	0.021	139

8.1.2 Internal uncertainties in the MIPS 24μm photometry

The minimum internal uncertainties for the MIPS 24μm photometry was established in a similar fashion as the IRAC photometry. Figure 8.2 shows a scatter plot of [4.5]-[24] vs. [4.5] and a histogram of the [4.5]-[24] color. Open circles represent stars with likely 24μm excesses, and the horizontal dashed line for a color of 0.0 is shown for reference. Evidently the scatter increases substantially for the fainter stars in this sample. Therefore, the minimum internal photometric uncertainties were evaluated in two brightness intervals after excluding stars with known 24μm excesses: brighter than [4.5]=7, and fainter than [4.5]=7. (The division should occur based on the MIPS 24μm magnitude, but it was deemed that the uncertainty in the 24μm photometry is larger enough at the fainter magnitudes stars that it was best to use the more precise IRAC 4.5μm photometry.)

Table 8.3 summarizes the mean and RMS of the observed [4.5]-[24] colors. The RMS in the color for stars fainter than [4.5]=7 is 2.9 times larger than the fainter stars. Given the uncertainty in the [4.5] magnitudes derived above, the typical MIPS 24μm uncertainty is 0.060 mag = 5.6% for stars brighter than [4.5] = 7.0 mag. For stars fainter than [4.5]=7.0, the RMS in the [4.5]-[24] color is 0.176 mag, which implies a [24] uncertainty of 0.200 mag = 16.2%.

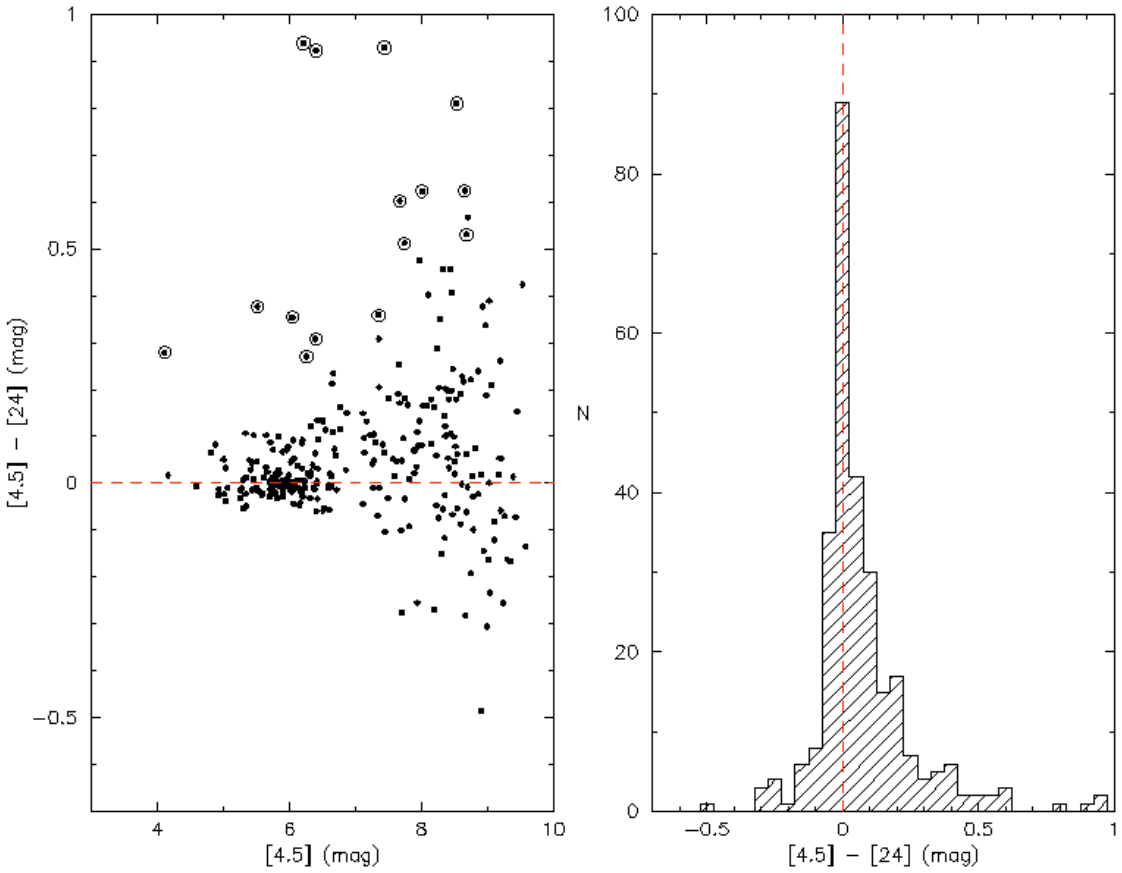

Figure 8.2: Plot of the observed [4.5]-[24] color vs. [4.5] magnitude (left panel) for stars in the V3.0 data release, and a histogram of the [4.5]-[24] color (right panel). Sources with open circles likely have MIPS 24μm excesses.

Table 8.2 summarizes the mean and RMS of the observed [4.5]-[24] colors. The RMS in the color for stars fainter than [4.5]=7 is 4.4 times larger than the fainter stars. Given the uncertainty in the [4.5] magnitudes derived above, the typical MIPS 24μm uncertainty is 0.044 mag = 4.0% for stars brighter than [4.5] = 7.0 mag. For stars fainter than [4.5]=7.0, the RMS in the [4.5]-[24] color is 0.200 mag, which implies a [24] uncertainty of 0.200 mag = 18.4%.

Table 8.3: Measured [4.5] - [MIPS24] colors

Magnitude Range	Mean color (mag)	RMS (mag)	Nstars
[4.5] < 7.0	0.022	0.061	140
[4.5] > 7.0	0.066	0.176	131

8.1.3 Internal uncertainties in the MIPS 70μm and 160μm photometry

The 70 and 160μm uncertainties are estimated from the coadded images by propagating the RMS fluctuations in the background annulus over the source aperture. Since the stellar photospheres have not detected at 70 and 160μm, the techniques used for IRAC and MIPS 24μm cannot be used to assess whether these computed uncertainties accurately reflect the internal uncertainties. Instead, the accuracy of the 70 and 160μm internal uncertainties were evaluated by considering the normalized residuals of the observed photometry with respect to the model photospheric fluxes (i.e. [observed flux - model flux] / sigma). For random noise, a histogram of the normalized residuals will have a gaussian distribution centered on zero with unit dispersion.

The left panel in Figure 8.3 presents histogram of the 70μm residuals for 260 FEPS sources, where the remaining 32 sources have a ratio >= 10.0 (29) sources or >= 10.0 -10 (3 sources) and are off scale on this figure. The left panel in Figure 3 shows the corresponding plot for 19 sources with 160μm photometry, where one source (HD 143006) is offscale. The 160μm source with a normalized residual of 5.8 is HD 105 and is considered to be a real excess. The source with a normalized residual of 7.7 is HD 104860. HD 105, HD 104860, HD 143006 were not used in the following analysis of the 160μm data.

The normalized residuals for the 70 and 160μm data have a dispersion of 3.3 and 1.0 respectively. The 70μm histogram is clearly larger than the expected value of 1.0. The origin of the increased dispersion is unclear, but may be related to fluctuations in the sky background that are not fully sampled in the sky annulus. These results suggest that the internal uncertainties in the MIPS 70μm photometry are underestimated by a factor of 3.3. The large dispersion could be attributed to other factors, but scaling the uncertainties in this manner is likely the most conservative approach. Therefore, the MIPS 70μm internal uncertainties have been increased in an ad hoc fashion by a factor 3.3. The 160μm uncertainties were not adjusted.

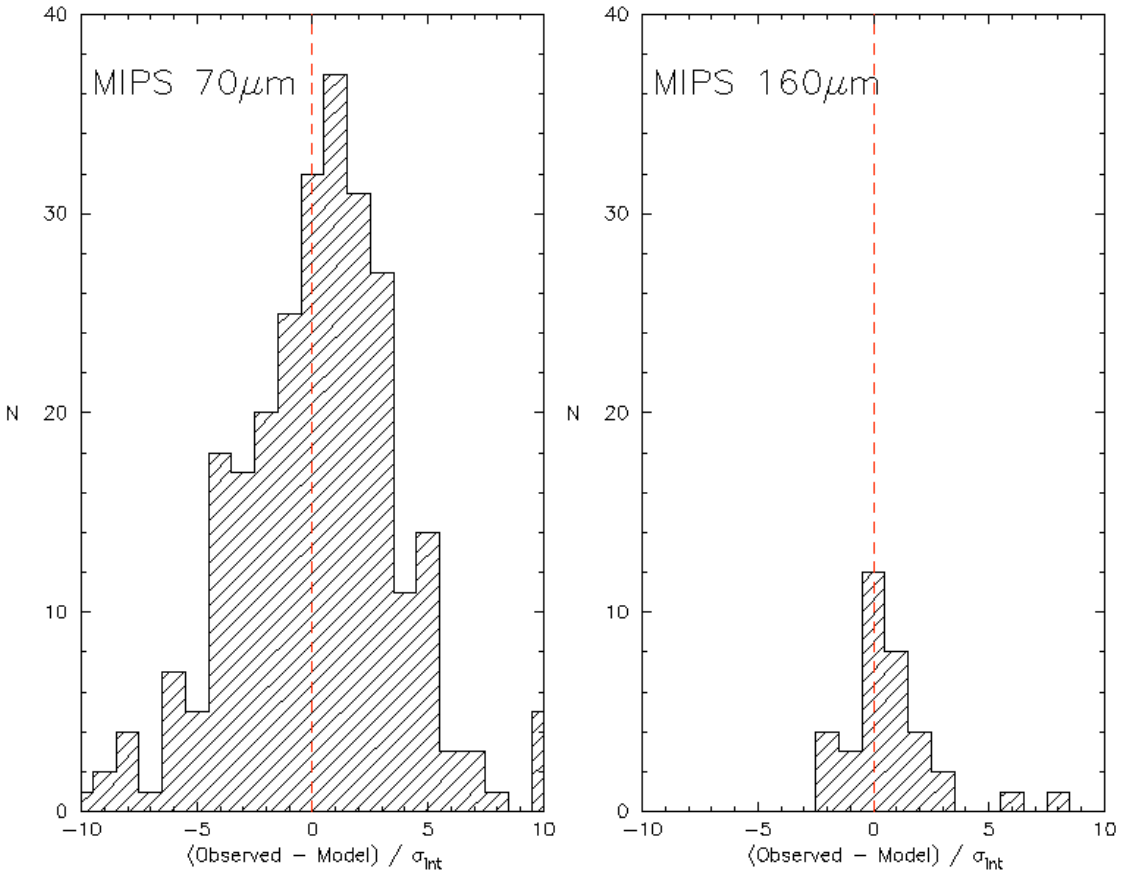

Figure 8.3: Plot of the ratio of observed to model flux normalized by the internal photometric uncertainty for 70μm (left panel) and 160μm (right panel) for stars in the V3.0 FEPS data release. Thirty-two stars have 70μm ratios greater off scale on this plot, and similarly, one 160μm star is offscale.

8.1.4 Calibration Uncertainties

Calibration uncertainties in the IRAC and MIPS 24μm photometry can be evaluated by comparing the observed photometry with the expected fluxes determined from the Kurucz model fitting (assuming there are no systematic errors in the fitting the Kurucz models). Figure 8.4 presents histograms of the difference between the observed photometry and model magnitudes for the stars in the FEPS release. Table 8.4 presents statistics on the mean and *rms* of the distributions. Calibration offsets cannot be derived for MIPS 70 and 160μm since in general the stellar photosphere was not detected in these bands. We note however that the FEPS target HD 13974 has been detected at 70μm, and the observed flux exceeds the photospheric flux by 16.3% ± 11.9%.

The scatter in the residual plots are larger than the IRAC color-color diagrams. This suggests the Kurucz model fitting is the dominant source of the scatter in the IRAC residual plots. In addition, there are systematic trends as a function of magnitude, which are not as apparent in the color-color diagrams. These systematic errors likely result from errors in the Kurucz models, but may also result from systematic errors common to the different IRAC channels. The systematic offsets present in Figure 8.4 likely represent upper limits to the calibration uncertainties.

Table 8.4: Difference Between Observed & Model Fluxes

Color	Magnitude Range	Mean (mag)	RMS (mag)	Nstars
IRAC 3.6	All	-0.091	0.042	286
IRAC 4.5	All	-0.054	0.053	286
IRAC 5.8	All	-0.098	0.024	5
IRAC 8.0	All	-0.073	0.050	286
MIPS 24	All	-0.037	0.144	271
	< 7.0	-0.009	0.071	140
	> 7.0	-0.068	0.189	131

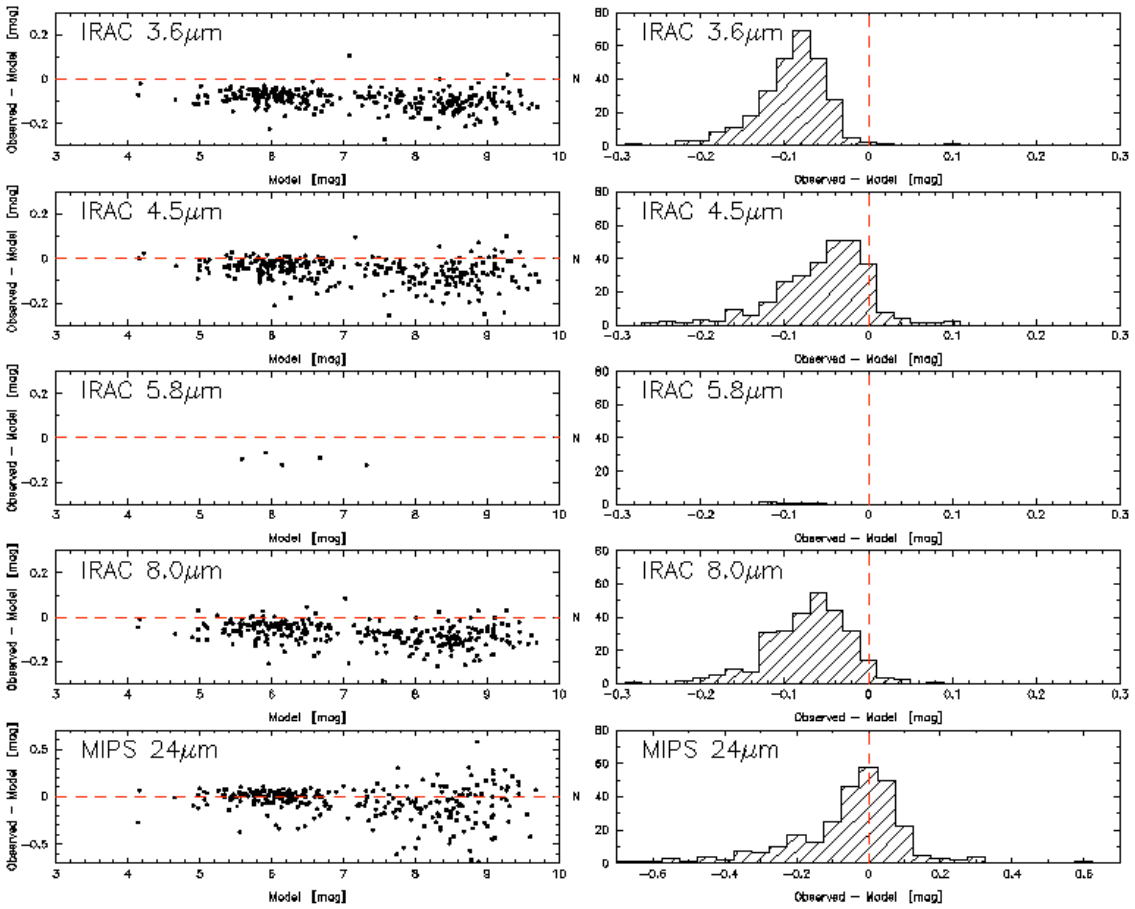

Figure 8.4: Plot of the difference between the observed fluxes and the model magnitudes for stars in the V3.0 data release (left panels), and histograms of the IRAC colors (right panels).

8.2 IRS Calibration

The details of the IRS low resolution spectral calibration strategy are given in Section 5.1. Figure 8.5 shows ratios between the observed fluxes and the model fluxes in IRS synthetic photometry bands for the 291 stars in the FEPS V3.0 delivery. There are systematic offsets in the calibration for the fainter stars in the sample, but the overall dispersion for each band is 5-10%. For the 33μm band, the majority of the outliers are stars that exhibit infrared excess emission.

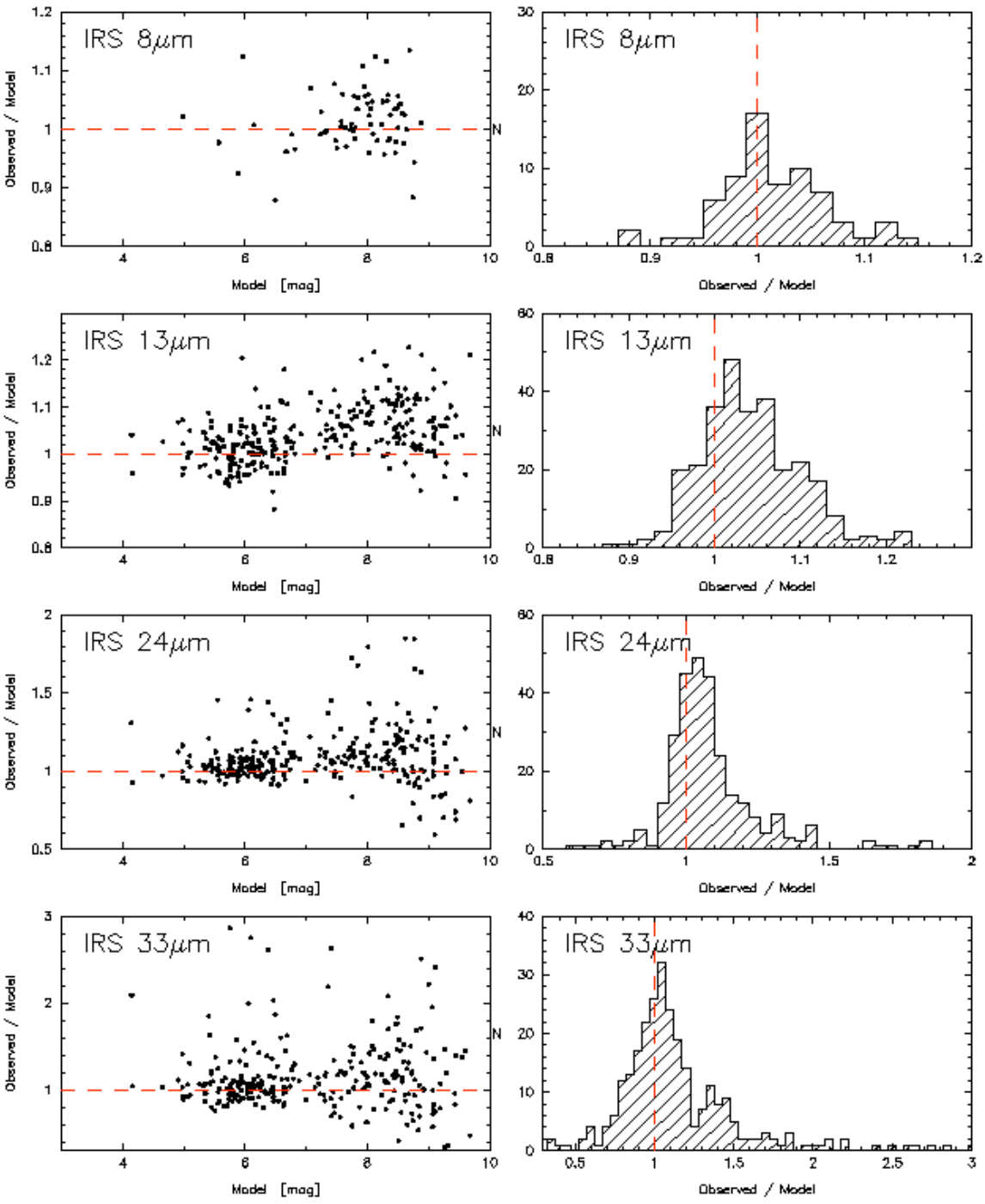

Figure 8.5: Plot of the ratio between the observed fluxes and the model fluxes in IRS synthetic photometry bands for the 291 stars in the FEPS V3.0 delivery. The left panels show the ratio *vs.* model magnitude, while the right panels show the histograms of the ratios.

8.3 Cross-Calibration

Comparison of the distributions of the IRS & IRAC 8μm band (4) and the IRS & MIPS 24μm band fluxes relative to the best fit Kurucz models for each object provide an assessment of the cross calibration between the three instruments. The IRS and IRAC across the 8mm band are consistent within 5%, while the IRS & MIPS across the 24μm band are consistent within 5%.

9 Ancillary Data Products

Ancillary 10μm, sub-millimeter and millimeter data has been obtained for several of our targets. These will appear in refereed journals and the relevant data tables will be linked from the FEPS Legacy archive.

9.1 10μm Photometry

Mid-IR imaging of selected members of the FEPS sample were obtained with MIRAC3 on the Magellan I telescope, with the LWS on the Keck I telescope, and with SpectroCam-10 (SC–10) on the Hale 5-meter telescope (Mamajek et al. 2004).

9.2 Millimeter and Sub-Millimeter Measurements

The millimeter and sub-millimeter observations and data are described in detail by Carpenter et al. (2004). Millimeter observations were obtained using the Owens Valley Radio Observatory (OVRO) millimeter-wave interferometer, 1.2mm observations were obtained for 89 stars using the 37-element SIMBA bolometer camera on the 15m Swedish-ESO Sub-millimeter Telescope (SEST), and submillimeter continuum observations at 350μm were obtained for 6 stars using the SHARC bolometer camera on the 10.4m telescope of the Caltech Sub-millimeter Observatory (CSO).

10 References

Carpenter, J.M., Wolf, S., Schreyer, K., Launhardt, R. & Henning, T. 2005, AJ, 129, 1049
Cohen, M., Megeath, S. T., Hammersley, P. L., Martiin-Luis, F. & Stauffer, J. 2003a, AJ, 125, 2645

Cohen, M., Wheaton, W. & Megeath, S. T. 2003b, AJ, 126, 1090

Hollenbach, D., et al. 2005, ApJ, 631, 1180

Mamajek, E.E., Meyer, M.R., Hinz, P.M., Hoffmann, W.F., Cohen, M., & Hora, J.L. 2004, ApJS, 612, 496.

Higdon, S.J.U., Devost, D., Higdon, J.L., Brandl, B.R., Houck, J.R., Hall, P., Barry, D., Charmandaris, V., Smith, J.D.T., Sloan, G.C. & Green, J. 2004, PASP, 116, 975

Schneider, G., & Stobie, E. 2002, ASP Conf. Ser. 281, Astronomical Data Analysis Software and System XI, ed. D. A. Bohlender, D. Durand, & T. H. Handley (San Francisco: ASP), p. 382

11 Appendix A

This appendix contains the parameter settings for the apphot photometry performed on the IRAC images in IRAF.

```
datapars
       (scale = 1.)             Image scale in units per pixel
     (fwhmpsf = **1*)           FWHM of the PSF in scale units
    (emission = yes)            Features are positive ?
       (sigma = INDEF)          Standard deviation of background in counts
     (datamin = INDEF)          Minimum good data value
     (datamax = INDEF)          Maximum good data value
       (noise = "poisson")      Noise model
     (ccdread = "")             CCD readout noise image header keyword
        (gain = "GAIN")         CCD gain image header keyword
   (readnoise = 0.)             CCD readout noise in electrons
        (epadu = 1.)            Gain in electrons per count
    (exposure = "SAMPTIME")     Exposure time image header keyword
     (airmass = "")             Airmass image header keyword
      (filter = "")             Filter image header keyword
     (obstime = "")             Time of observation image header keyword
       (itime = 1.)             Exposure time
    (xairmass = INDEF)          Airmass
     (ifilter = "INDEF")        Filter
       (otime = "INDEF")        Time of observation
        (mode = "ql")

photpars
   (weighting = "constant")     Photometric weighting scheme for wphot
   (apertures = "2,10")         List of aperture radii in scale units
        (zmag = 25.)            Zero point of magnitude scale
     (mkapert = no)             Draw apertures on the display
        (mode = "ql")

fitskypars
  (salgorithm = "median")       Sky fitting algorithm
     (annulus = 10.)            Inner radius of sky annulus in scale units
    (dannulus = 32.)            Width of sky annulus in scale units
    (skyvalue = 0.)             User sky value
    (smaxiter = 10)             Maximum number of sky fitting iterations
     (sloclip = 0.)             Lower clipping factor in percent
     (shiclip = 0.)             Upper clipping factor in percent
    (snreject = 50)             Maximum number of sky fitting rejection iterati
   (sloreject = 3.)             Lower K-sigma rejection limit in sky sigma
   (shireject = 3.)             Upper K-sigma rejection limit in sky sigma
        (khist = 3.)            Half width of histogram in sky sigma
     (binsize = 0.1)            Binsize of histogram in sky sigma
      (smooth = no)             Boxcar smooth the histogram
       (rgrow = 0.)             Region growing radius in scale units
       (mksky = no)             Mark sky annuli on the display
        (mode = "ql")

centerpars
  (calgorithm = "gauss")        Centering algorithm
        (cbox = 5.)             Centering box width in scale units
  (cthreshold = 3.)             Centering threshold in sigma above background
  (minsnratio = 1.)             Minimum signal-to-noise ratio for centering alg
    (cmaxiter = 10)             Maximum number of iterations for centering algo
    (maxshift = 1.5)            Maximum center shift in scale units
       (clean = no)             Symmetry clean before centering ?
      (rclean = 1.)             Cleaning radius in scale units
       (rclip = 2.)             Clipping radius in scale units
      (kclean = 3.)             Rejection limit in sigma
    (mkcenter = no)             Mark the computed center on display ?
        (mode = "ql")
```

12 (Incomplete) Acronym List

AOR — Astronomical Observation Request
AOT — Astronomical Observation Template
ASCII — American Standard Code for Information Interchange
BCD — Basic Calibrated Data
BQD — Browse Quality Data
DCE — Data Collection Event
DN — Data Number
FITS — Flexible Image Transport System
FPA — Focal Plane Array
Si:As — Silicon detectors doped with Arsenic
GTO — Guaranteed Time Observer
IRAC — Infrared Array Camera
IRS — Infrared Spectrograph
MIPS — Multiband Imaging Photometer for SIRTF
PSF — Point Spread Function
SED — Spectral Energy Distribution
SSC — Spitzer Science Center